Received: 30 May 2022 | Revised: 15 February 2023 | Accepted: 18 April 2023

DOI: 10.1002/ldr.4730

RESEARCH ARTICLE

WILEY

Holocene deglaciation of the northern Fildes Peninsula, King George Island, Antarctica

Marc Oliva[1] | David Palacios[2] | José M. Fernández-Fernández[2] | Marcelo Fernandes[3] | Irene Schimmelpfennig[4] | Gonçalo Vieira[3] | Dermot Antoniades[5] | Augusto Pérez-Alberti[6] | Julia García-Oteyza[1] | ASTER TEAM[4,7]

[1]Department of Geography, Universitat de Barcelona, Catalonia, Spain

[2]Department of Geography, Universidad Complutense de Madrid, Madrid, Spain

[3]Centre for Geographical Studies, IGOT, Lisbon, Universidade de Lisboa, Lisboa, Portugal

[4]Aix-Marseille Université, CNRS, IRD, INRAE, Coll France, UM 34 CEREGE, Aix-en-Provence, France

[5]Department of Geography & Centre for Northern Studies, Université Laval, Quebec City, Quebec, Canada

[6]Cross-Research in Environmental Technologies (CRETUS), Universidade de Santiago Compostela, Santiago de Compostela, Spain

[7]Consortium: Georges Aumaître, Karim Keddadouche

Correspondence
Marc Oliva, Department of Geography, Universitat de Barcelona, Montalegre 6-8, 3r floor, 08001 Barcelona, Spain.
Email: marcoliva@ub.edu

Funding information
Universidade de Lisboa; Fundação para a Ciência e Tecnologia of Portugal, Grant/Award Number: 02/SAICT/2017 – 32002; Ministerio de Economía y Competitividad, Spain, Grant/Award Number: CTM2016-77878-P; Antarctic, Arctic, Alpine Environments, Grant/Award Number: 2017-SGR-1102; Agència de Gestió d'Ajuts Universitaris i de Recerca of the Government of Catalonia; ZEPHYRUS (Climate Change and Environmental Systems); College on Polar and Extreme Environments (Polar2E); NEOGREEN, Grant/Award Number: PID2020-113798GB-C31; Spanish Ministerio de Economía y Competitividad; Ramón y Cajal Program, Grant/Award Number: RYC-2015-17597; Marcelo Fernandes by a PhD fellowship of the Fundação para a Ciência e Tecnologia of Portugal, Grant/Award Number: UIDB/00295/2020; INSU/CNRS

Abstract

The timing and magnitude of Holocene glacial oscillations in most currently ice-free areas of Antarctica remain unknown. This work focuses on the recent deglaciation in the northern sector of the Fildes Peninsula, King George Island, northern Antarctic Peninsula. The ice cap covering ca. 90% of the island has receded since the Last Glacial Maximum and exposed ca. 29 km^2 of ice-free land. We reconstruct its glacial history based on a dataset of 12 ^{36}Cl exposure ages obtained through cosmic-ray exposure (CRE) dating of moraine boulders, polished surfaces and erratic boulders surrounding the peninsula's northern plateau. Results reveal that the deglaciation of the northern Fildes Peninsula took place during the Holocene Thermal Maximum at 7–6 ka, when warm conditions promoted a massive glacial retreat. The present arrangement of ice-free areas was in place by 6 ka. Small cirque moraines suggest the subsequent occurrence of favourable climate conditions for glacial expansion fed by intense snow deflation at 4.6 and 1 ka at the foot of the northern plateau. The deglaciation pattern of the Fildes Peninsula resulted from the combined shrinkage of different ice masses, rather than of the long-term retreat of the King George Ice Cap. No evidence of glacier expansion during more recent cold periods (i.e. the Little Ice Age) was found. These results fit well with regional deglacial histories inferred from lacustrine sediments and raised beaches and complement the existing chronological

framework to help better understand the peninsula's Holocene geoecological dynamics.

KEYWORDS
Antarctica, cosmic-ray exposure dating, deglaciation, Fildes Peninsula, Holocene Thermal Maximum

1 | INTRODUCTION

The large variations in the volume of ice stored in the polar regions during the Quaternary played a key role in the dynamics of the global climate system. Following the maximum ice extent of the last glacial cycle at 26–19 ka (Last Glacial Maximum, LGM) (Clark et al., 2009), variations in ice accumulation in the high latitudes have been controlled by the prevailing climate conditions. The magnitude of climatic and environmental changes was particularly notable during the last deglaciation (Termination-1; 19–11 ka), when high deglaciation rates accelerated the appearance of ice-free environments and the reconfiguration of landscapes in the polar and mountain regions, particularly in the Northern Hemisphere.

In contrast to Termination-1, ice sheets, ice caps and mountain glaciers in the polar regions have remained relatively stable since the onset of the current interglacial (Briner et al., 2020; Noble et al., 2020). Glacial advances and retreats have been small in response to prevalent colder and warmer phases. Notwithstanding, Holocene glacial oscillations have had a prominent role in the configuration of present-day ice-free landscapes: the age of deglaciation controls geoecological dynamics, including the intensity of geomorphic processes, permafrost aggradation/degradation, type and extent of vegetation cover, degree of soil development and even the biogeographic distributions of fauna (Ruiz-Fernández et al., 2019).

Only <0.5% of the total area of the Antarctic continent is ice free (between 32,000–60,000 km^2; Burton-Johnson et al., 2016) and only a small proportion of the land surface has become exposed during the Holocene (Nývlt et al., 2020). Indeed, most coastal ice-free environments in Maritime Antarctica (Bentley et al., 2009; Giralt et al., 2020; Ó Cofaigh et al., 2014), as well as several nunataks across the continent (Small et al., 2019), were deglaciated during the Holocene Thermal Maximum (HTM) that occurred globally at ca. 9–5 ka (Renssen et al., 2009; Renssen et al., 2012). In the mildest region of Antarctica, the northern Antarctic Peninsula (AP), where present-day mean annual air temperatures (MAAT) average ca. −2 and −3°C at sea level and positive summer temperatures favour intense ablation, low amplitude changes in temperature and precipitation during the Holocene must have induced significant fluctuations of AP ice sheets, including the small ice caps extending across the surrounding islands as well as the existing mountain glaciers (Oliva, Serrano, Gómez-Ortiz, González-Amuchastegui, Nieuwendam, Palacios, Pérez-Alberti, et al., 2016).

In the South Shetland Islands (SSI), located in the north-west AP, glaciers currently extend over 86–95% of the land surface of the major islands (RGI Consortium, 2017). The shrinking of ice caps during the Holocene has exposed coastal lowlands along the margins of the islands, which constitute some of the greatest hotspots of biodiversity of the entire continent (Convey et al., 2020). Spatio-temporal patterns of glacial retreat in these islands are of major importance for understanding the factors and processes controlling present-day geoecological dynamics in ice-free environments. However, there is a lack of chronological control of these patterns in most regions of the AP. The first deglacial chronologies were based on radiocarbon dating of organic fragments preserved in lacustrine and marine sediments as well as in raised marine terraces (e.g., Björck et al., 1991; Watcham et al., 2011), which were recently complemented by the increasing use of cosmic-ray exposure (CRE) dating.

The highest areas in the SSI were deglaciated during the LGM and Termination-1, with deglaciation accelerating between ca. 19.5 and 13 ka and exposing the lowest portions of the nunataks next to the present-day edges (Fernández-Fernández et al., 2021) The highest exposed summits on King George Island (KGI) were also exposed by this time (Seong et al., 2009). Only small changes in ice thinning have occurred since ca. 13 ka (Fernández-Fernández et al., 2021); however, these small vertical changes were accompanied by extensive horizontal retreats of nearby ice masses. For example, the deglaciation of the Fildes Peninsula occurred during the HTM, and advances of Collins Glacier after 7 ka have been limited (^{10}Be dating; Heredia Barión, 2019). This chronology is similar to that inferred from other ice-free areas of KGI, such as the Barton and Potter peninsulas, where deglaciation began at ca. 8 and 7.8 ka cal BP, respectively (Heredia Barión, 2019; Oliva et al., 2019). Since the Mid-Holocene, any glacial advances must have been small and mostly confined to present-day glacier forelands (Oliva & Ruiz-Fernández, 2017), although they often lack temporal constraint. Reconstructed chronologies have mostly focused on indirect records, such as raised beaches or lacustrine sediments, and did not date glacial landforms directly. Further glacial evidence of Neoglacial oscillations in other areas of the SSI is therefore needed to better understand the regional patterns of Holocene glaciation in the AP region.

The objective of this work is to examine the spatial and temporal patterns of the last stages of the deglaciation of the Fildes Peninsula, namely at the northern plateau, located close to the Collins Glacier (Figure 1). To achieve this goal, we will address the following questions:

- Did the last glacial retreat on the Fildes Peninsula occur during the Holocene?
- How did the warm conditions prevailing during the HTM affect the King George Ice Cap (Figure 1) and local glaciers?

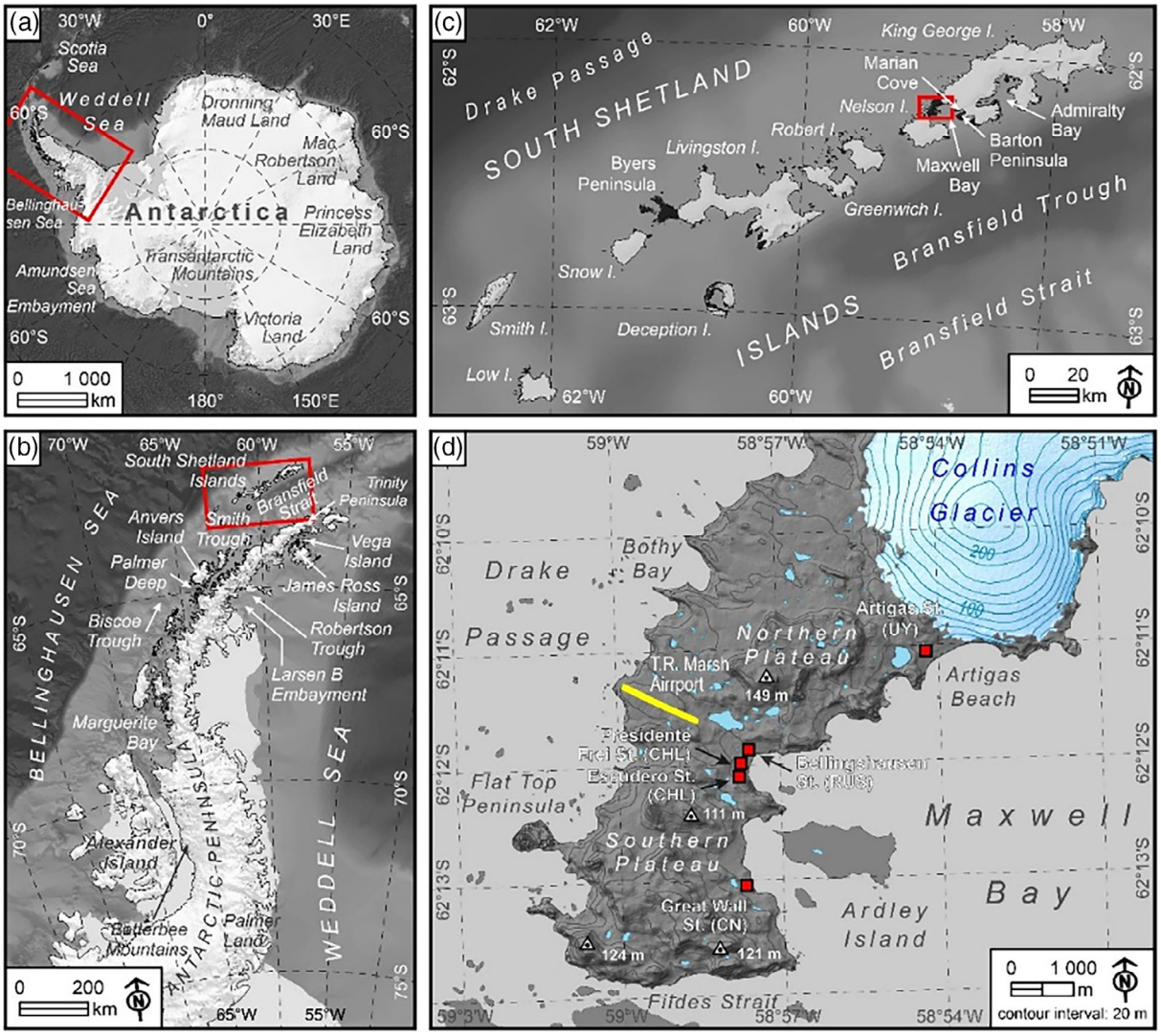

FIGURE 1 Location of the AP (a), the SSI (b), KGI (c) and the Fildes Peninsula with the local names mentioned in this study and the airstrip in yellow (d). [Colour figure can be viewed at wileyonlinelibrary.com]

- Is there any Neoglacial evidence in the glacial geomorphological record?

2 | STUDY AREA

KGI is the largest island of the SSI archipelago with a total surface area of 1124 km^2, of which 83.3% is covered by glaciers (Shahateet et al., 2021) (Figure 1). The Fildes Peninsula sits at the SW tip of the island and is the second largest ice-free area in the SSI (29 km^2; Michel, Schaefer, López-Martínez, et al., 2014). The peninsula is one of the most heavily humanised areas in Antarctica: it hosts six research stations, several refuges and huts as well as an important concentration of human infrastructure (airport, roads, fuel tanks, etc.). An Antarctic Specially Protected Area (ASPA) incorporates eight fragmented spaces across the ice-free area of the Fildes Peninsula (ASPA No. 125; ATCM, 2009).

The climate of KGI is typical of Maritime Antarctica, with slightly negative MAAT and relatively high precipitation values as compared with the rest of the Antarctica (Gonzalez & Vasallo, 2020). Bellingshausen Station has a MAAT of −2.5°C (1948–2016) and a mean annual precipitation of 698 mm (1968–2016) (Pasik et al., 2021). Vegetation cover is sparse, but this includes a rich variety of mosses and grasses, mostly concentrated on marine terraces (Henriques et al., 2018). The unvegetated terrain is composed mainly of basalts and basaltic andesites of Mesozoic and Cenozoic age (Machado et al., 2005), and is prone to intense physical weathering processes, with frequent freeze–thaw cycles enhancing frost shattering. As in the rest of the ice-free areas of the SSI, the Fildes Peninsula experiences intense periglacial dynamics with shallow and poorly developed soils affected by intense cryogenic processes (López-Martínez et al., 2012; Michel, Schaefer, López-Martínez, et al., 2014). Permafrost is sporadic or discontinuous up to 20–40 m a.s.l. and becomes continuous at higher elevations (Bockheim et al., 2013; Vieira et al., 2010), with an active layer that can reach 1.15 m thickness (Michel, Schaefer, Simas, et al., 2014).

The current ice-free area is the result of the northwards post-LGM glacial retreat of the King George Ice Cap. This deglaciation age

TABLE 1 Geographic sample locations, topographic shielding factor and sample thickness.

Sample name	Feature	Latitude (DD)	Longitude (DD)	Elevation (m a.s.l.)[a]	Topographic shielding factor	Neutrons spallation rate Sλ (P)	Muon capture rate Mλ (P)	Thickness (cm)
Southern plateau								
ART-23	Polished surface	−62.1909	−58.9516	46	0.9963	1.2757	1.1193	3.2
ART-24	Polished surface	−62.1906	−58.9512	50	0.9941	1.2808	1.1215	3.0
ART-25	Erratic boulder	−62.1953	−58.9436	28	0.9996	1.2513	1.1089	4.5
ART-26	Erratic boulder	−62.1960	−58.9471	43	0.9995	1.2708	1.1172	3.5
ART-27	Erratic boulder	−62.1931	−58.9482	43	0.9996	1.2708	1.1173	3.6
ART-28	Erratic boulder	−62.1942	−58.9473	41	0.9990	1.2683	1.1162	2.8
Northern plateau								
ART-32	Polished surface	−62.1764	−58.9697	39	0.9998	1.2659	1.1152	4.2
ART-33	Polished surface	−62.1780	−58.9671	49	0.9999	1.2789	1.1207	4.0
ART-34	Polished surface	−62.1814	−58.9596	51	0.9958	1.2811	1.1217	4.5
ART-35	Moraine boulder	−62.1823	−58.9579	61	0.9847	1.2958	1.1279	4.2
ART-36	Moraine boulder	−62.1823	−58.9578	61	0.9850	1.2958	1.1279	3.9
ART-37	Moraine boulder	−62.1784	−58.9551	53	0.9937	1.2847	1.1232	5.0

[a]Elevation data were taken from the TanDEM-X and corrected to orthometric by applying the Earth Gravitational Model 2008 (EGM08).

also explains the formation of the sequence of marine terraces around the island due to glacio-isostatic rebound (Fretwell et al., 2010), the abundant lakes and lagoons (Fretwell et al., 2010), as well as the colonisation of the flora and the settlement of penguin colonies (Tatur et al., 2004). The long-term rate of glacial retreat has accelerated in recent decades (Rückamp et al., 2011) in response to the rapid warming recorded during the second half of the 20th century in the AP region (Turner et al., 2005). Most glacier outlets across the island have recorded significant retreats (Pasik et al., 2021), including the Collins Glacier on the NE fringe of the Fildes Peninsula (Petsch et al., 2020).

Topographically, the Fildes Peninsula is characterised by two main plateaus, in its northern and southern sectors, that are surrounded by several lower rocky outcrops and marine terraces at elevations between 2 and 18.5 m a.s.l. (Fretwell et al., 2010; Figure 1). The northern plateau extends over ca. 2 km^2 and is located at 0.7–3 km from the current glacial front; the highest points there reach 145–155 m and adjoin the lowlands abruptly via steep slopes, particularly on the northern and western sides. By contrast, the southern plateau includes rougher terrain, with several peaks exceeding 150 m and hills dissected by valleys; it extends over 7 km^2 and is 4–8 km from the glacier front. At 11–10 ka, glaciers may have covered most of the current ice-free land surface of the peninsula, which was gradually exposed during the Holocene (Ingólfsson et al., 1998; Tatur et al., 2004). The coves alongside Maxwell Bay show different elevations of raised beaches from 18–21 m a.s.l. down to the current sea level, indicative of past deglaciation patterns in the region (Fretwell et al., 2010; Hall, 2010).

3 | METHODOLOGY

We carried out fieldwork on the Fildes Peninsula in February 2019 with two main objectives: (i) to conduct a geomorphological survey of the principal landforms, and (ii) to collect rock samples from glacial landforms in order to reconstruct the spatio-temporal pattern of deglaciation. Based on the results of the geomorphological survey, we collected a total of 12 samples from the surficial layer of basaltic glacially polished rock outcrops (3–5 cm thick; Table 1) and moraine and erratic boulders using a hammer and a chisel (Figure 2). Flat and gentle rock faces were selected preferentially to sharp crests and steep hillsides, with the aim of ensuring optimal cosmic-ray reception. We were unable to carry out field measurements of the horizon due to poor weather conditions during sampling (i.e., limited visibility). As such, to geometrically correct for partial shielding by the surrounding

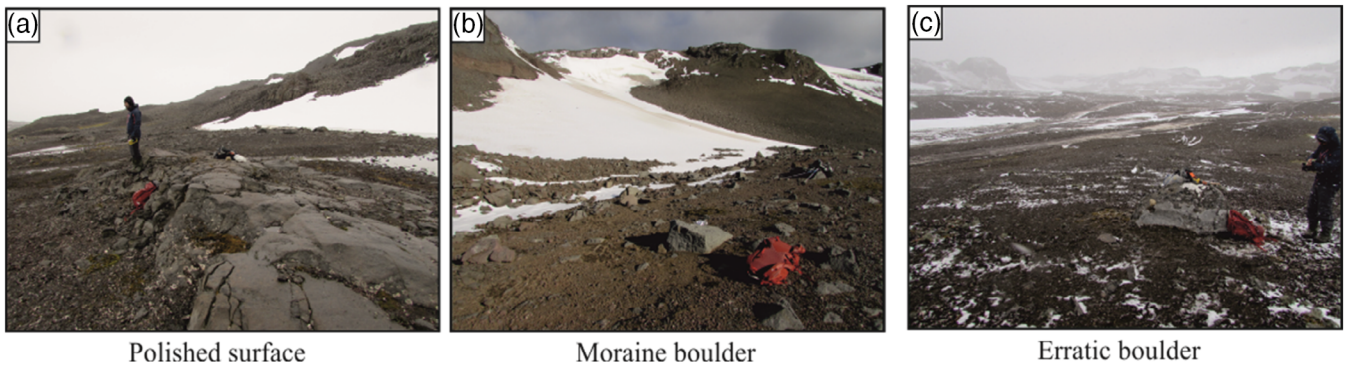

FIGURE 2 Examples of the different glacial records sampled in this study. [Colour figure can be viewed at wileyonlinelibrary.com]

topography, we calculated the topographic shielding factor using the ArcGIS toolbox developed by Li (2018), which implements the well-known routines explained in Dunne et al. (1999).

Samples were crushed and sieved to retain the 0.25–1.0 mm fraction in the Physical Geography Laboratory of the Universidad Complutense de Madrid (Spain). Due to the basaltic nature of the samples, the cosmogenic nuclide ^{36}Cl was chosen to perform cosmic-ray exposure (CRE) dating. Rock samples did not have abundant feldspar minerals, and therefore we followed chemical procedures for the ^{36}Cl extraction of whole rock based on Schimmelpfennig et al. (2011). Chemical sample processing was conducted in the "Laboratoire National des Nucléides Cosmogéniques" (LN_2C) of the "Centre Européen de Recherché et d'Enseignement des Géosciences de l'Environnement" (CEREGE; Aix-en-Provence, France). Prior to chemical processing, we took aliquots of untreated bulk samples to determine the sample composition (i.e., concentration of major/trace elements; Table 2). Firstly, initial weights of 120 g were rinsed with ultrapure water through shaking for 3 h to remove dust and fine particles. To remove atmospheric ^{36}Cl and any potential chlorine-rich ground mass, between 40 and 50% of the sample mass was dissolved by leaching with a mixture of diluted nitric acid (10% HNO_3) and concentrated hydrofluoric acid (48% HF). After this step, the remaining leached sample mass was rinsed and dried, and 2-g aliquots were taken to determine the major element concentrations in the target fraction (Table 3). Analysis of the aliquots was performed at the "Service d'Analyse des Roches et des Minéraux" (SARM, CRPG, Nancy, France). About 300 µL of an in-house manufactured ^{35}Cl carrier (spike: 261018, 6.019 ± 0.115 Cl g^{-1}, $^{35}Cl/^{37}Cl$ ratio 296.9 ± 3.6) were then added to the samples for isotopic dilution (Ivy-Ochs et al., 2004). For the total dissolution of the samples, we added a mixture of 9 mL 10% HNO_3 and 4.5 mL 48% HF per gram, and finally, samples were shaken for 48 h to complete the dissolution. After total dissolution, the samples were centrifuged to separate the dissolved sample from undissolved residues and fluoride complexes (CaF_2, gel). Exactly 2 mL of a 10% silver nitrate ($AgNO_3$) was added to precipitate the chlorine of the liquid solution as silver chloride (AgCl). The samples were then stored for 48 h in a dark place to complete precipitation and allow the AgCl precipitate to settle. We next extracted the supernatant solution by using a peristaltic pump, thus avoiding any disturbance of the precipitate. Later, to reduce isobaric interference of ^{36}S during measurements in the accelerator mass spectrometer (AMS), the first AgCl precipitate was re-dissolved in dilute ammonia and 1 mL of a saturated solution of barium nitrate ($Ba(NO_3)_2$) was added to remove sulphur in the form of barium sulphate ($BaSO_4$). The removal of $BaSO_4$ was achieved through filtration of the supernatant solution with a syringe and an acrodisc filter. Subsequently, AgCl was precipitated again by adding 3–4 mL of diluted HNO_3 (1:1 vol.). Finally, the precipitate was collected after centrifuging and was rinsed and dried in the oven at 80°C for 48 h.

The final AgCl targets were analysed at the "Accelérateur pour les Sciences de la Terre, Environnement et Risques" (ASTER) AMS facility at CEREGE to measure the specific isotope ratios of $^{35}Cl/^{37}Cl$ and $^{36}Cl/^{35}Cl$, from which the ^{36}Cl concentrations (in atoms g^{-1}) were inferred (Table 4). The measurement of these ratios was normalised to the in-house standard SM-CL-12 with an assigned $^{36}Cl/^{35}Cl$ ratio value of 1.428 ± 0.021 10^{-12} (Merchel et al., 2011) and assuming a natural ratio of $^{35}Cl/^{37}Cl = 3.127$. Analytical 1σ uncertainties include uncertainties in AMS counting statistics.

^{36}Cl exposure ages were calculated using the Excel™ spreadsheet for in situ calculations proposed by Schimmelpfennig et al. (2009) because of its flexibility in the input of different ^{36}Cl production rates from the spallation of several elements. The ^{36}Cl production rates—referenced to sea level and high latitude; SLHL—from the spallation of Ca, K, Ti and Fe used for the calculations were: 42.2 ± 4.8 ^{36}Cl (g Ca)$^{-1}$ year^{-1} (Schimmelpfennig et al., 2011), 148.1 ± 7.8 ^{36}Cl (g K)$^{-1}$ year^{-1} (Schimmelpfennig et al., 2014), 13 ± 3 ^{36}Cl (g Ti)$^{-1}$ year^{-1} (Fink et al., 2000) and 1.9 ± 0.2 atoms ^{36}Cl (g Fe)$^{-1}$ year^{-1}, respectively. The rate used for epithermal neutron production from fast neutrons in the atmosphere at the land/atmosphere interface was 696 ± 185 neutrons (g air)$^{-1}$ year^{-1} (Marrero et al., 2016). The high energy neutron attenuation length applied was 160 g cm^{-2}. The density is assumed to be 2.4 g cm^{-3}. The elevation-latitude scaling factors were based on the time invariant scheme ("St"; Stone, 2000).

Ca spallation is the most dominant in situ ^{36}Cl production reaction in our samples, and the air pressure at the sampling sites needed to be corrected given that the production rate of Schimmelpfennig et al. (2011) was calibrated at Etna volcano, that is, in a region with a

TABLE 2 Chemical composition of the bulk rock samples before chemical treatment.

Sample name[a]	CaO (%)	K_2O (%)	TiO_2 (%)	Fe_2O_3 (%)	SiO_2 (%)	Na_2O (%)	MgO (%)	Al_2O_3 (%)	MnO (%)	P_2O_5 (%)	Cl (ppm)	Li (ppm)	B (ppm)	Sm (ppm)	Gd (ppm)	Th (ppm)	U (ppm)
Southern plateau																	
ART-23	10.158	0.191	0.869	9.378	47.990	3.345	3.560	20.867	0.157	0.110	27	5.200	2	2.555	2.514	0.644	0.216
ART-28	10.445	0.708	0.798	7.828	49.060	3.463	3.534	21.067	0.243	0.230	42	6.270	2	5.197	4.507	1.736	0.559
Northern plateau																	
ART-33	10.300	0.361	0.755	9.256	47.480	2.726	5.351	19.280	0.166	0.120	51	5.930	2	2.300	2.323	0.568	0.071
ART-34	9.738	0.724	0.757	9.127	51.130	3.418	4.042	19.033	0.163	0.150	26	6.800	4	2.980	2.781	1.258	0.384
ART-35	8.844	0.340	0.802	8.401	48.480	3.644	4.067	19.248	0.159	0.120	48	5.810	2	2.325	2.362	0.722	0.139

[a]In the case of samples with no available information on bulk composition, it is applied as it follows: ART-23 (ART-24), ART-28 (ART-25, ART-26, ART-27), ART-33 (ART-32), ART-34 (ART-37), ART-35 (ART-36).

different atmospheric setting than that of our study region. The SSI, according to their latitude, is affected by a permanent subpolar low-pressure system, which influences the cosmic-ray particle flux such that the production rate is enhanced. Any long-term atmospheric pressure anomaly should be considered, at least for Holocene exposure periods (Dunai, 2010). As such, we corrected the atmospheric pressure at the sampling sites by running the ERA40 atmosphere model (Uppala et al., 2005) using the MATLAB function "ERA40.mat" (Lifton et al., 2014). We did not use the specific Antarctic atmosphere model (Stone, 2000), as the atmosphere in continental Antarctica is affected by the air flow over the ice sheet, and this modifies the elevation/air pressure relationship in the opposite way (cold high pressure at surface level). The difference between using the results obtained from the ERA40 model and the air pressure values from nearby weather stations (e.g., Bellinghausen, 62.2° S, 58.9° W, 16 m a.s.l.; 991.05 hPa) is negligible, and thus the use of the ERA40 model in this area can be considered valid.

In order to identify potential outliers according to statistical criteria, we applied a chi-squared test to sample populations corresponding to the same geomorphological units, including the analytical uncertainties of the CRE results (Ward & Wilson, 1978). Uncertainties in exposure ages presented hereafter include the error on the AMS measurements (internal uncertainty; 1σ) as well as that derived from the scaling and production rate uncertainties (Table 4), unless otherwise stated. No erosion/snow/glacial isostatic adjustment correction was made for the age calculations.

4 | RESULTS

The glacial features that we identified in the northern sector of the Fildes Peninsula provided numerous insights about the last retreat of the King George Ice Cap. We present 12 ^{36}Cl CRE ages of glacial landforms that provide the chronological framework for the last stages of deglaciation in the northern ice-free area of this peninsula.

4.1 | Geomorphology

The central sector of the Fildes Peninsula is dominated by its northern plateau, which is characterised by relatively flat relief at ~110–130 m a.s.l., and includes several lakes occupying overdeepened basins (Figure 1). The highest peaks (145–155 m) are composed of resistant basaltic rocks and are situated on the SW fringe of the plateau. No moraine systems exist on the plateau following deglaciation, and the most notable geomorphological features are defined by frost shattering that has completely dismantled the exposed bedrock. After a detailed field survey across the plateau, we were unable to find any original glacially polished surfaces, and therefore no samples for CRE dating were collected.

The northern plateau is surrounded by steep hillsides along its N and W edges and descends gradually towards the NE–SE flanks that connect gently with the most recent moraine system. This eastern

TABLE 3 Oxide concentrations of the ^{36}Cl target elements (Ca, K, Ti and Fe) and the other major elements (Si, Al, Mn, Mg and Na) determined in splits taken after the chemical pre-treatment (acid leaching).

Sample name	CaO (%)	K_2O (%)	TiO_2 (%)	Fe_2O_3 (%)	SiO_2 (%)	Al_2O_3 (%)	MnO (%)	MgO (%)	Na_2O (%)
Southern plateau									
ART-23	6.78 ± 0.34	0.12 ± 0.03	0.77 ± 0.15	6.19 ± 0.62	63.51 ± 1.27	12.32 ± 0.25	0.13 ± 0.03	2.57 ± 0.26	2.45 ± 0.25
ART-24	6.03 ± 0.30	0.17 ± 0.04	0.91 ± 0.18	7.23 ± 0.72	64.54 ± 1.29	10.89 ± 0.22	0.15 ± 0.03	2.50 ± 0.25	2.30 ± 0.23
ART-25	6.65 ± 0.33	1.03 ± 0.10	0.67 ± 0.13	4.15 ± 0.42	66.21 ± 1.32	12.90 ± 0.26	0.19 ± 0.04	2.11 ± 0.21	2.84 ± 0.28
ART-26	6.51 ± 0.33	1.31 ± 0.13	0.95 ± 0.19	7.08 ± 0.71	61.93 ± 1.24	13.21 ± 0.26	0.19 ± 0.04	3.28 ± 0.33	2.95 ± 0.29
ART-27	6.93 ± 0.35	0.64 ± 0.13	0.78 ± 0.16	4.87 ± 0.49	65.25 ± 1.31	13.53 ± 0.27	0.19 ± 0.04	1.94 ± 0.19	2.56 ± 0.26
ART-28	6.81 ± 0.34	0.46 ± 0.11	0.70 ± 0.14	4.69 ± 0.47	66.54 ± 1.33	11.94 ± 0.24	0.16 ± 0.03	2.11 ± 0.21	2.24 ± 0.22
Northern plateau									
ART-32	8.56 ± 0.43	0.22 ± 0.05	0.76 ± 0.15	8.29 ± 0.83	59.70 ± 1.19	13.33 ± 0.27	0.16 ± 0.03	4.26 ± 0.43	1.92 ± 0.19
ART-33	7.41 ± 0.37	0.19 ± 0.05	0.91 ± 0.18	9.31 ± 0.93	60.67 ± 1.21	10.41 ± 0.21	0.18 ± 0.04	4.9 ± 0.49	1.88 ± 0.19
ART-34	5.88 ± 0.29	0.72 ± 0.14	0.9 ± 0.18	8.83 ± 0.88	63.99 ± 1.28	10.67 ± 0.21	0.18 ± 0.04	3.67 ± 0.37	2.63 ± 0.26
ART-35	5.84 ± 0.29	0.21 ± 0.05	1.0 ± 0.10	8.41 ± 0.84	61.83 ± 1.24	10.72 ± 0.21	0.20 ± 0.04	3.18 ± 0.32	2.46 ± 0.25
ART-36	6.31 ± 0.32	0.13 ± 0.03	0.85 ± 0.17	7.97 ± 0.80	63.59 ± 1.27	10.54 ± 0.21	0.17 ± 0.03	3.48 ± 0.35	2.12 ± 0.21
ART-37	4.14 ± 0.62	0.58 ± 0.12	0.87 ± 0.17	10.25 ± 1.02	64.44 ± 1.29	6.31 ± 0.63	0.16 ± 0.03	2.63 ± 0.26	1.32 ± 0.13

fringe between the plateau and the moraine is composed of fine-grained sediments defining a periglacial landscape with sorted circles, stone stripes, solifluction lobes and mud flows. We observed several parallel ridges, and small lobate-shaped arches that define proglacial areas with a large amount of recent sediments deposited by glacier meltwater, which indicate that the N–S moraine enclosing the Collins Glacier is polygenic (Figure 3).

On the NW and S-SE fringes of the plateau, there is scattered geomorphic glacial evidence in the form of glacially polished bedrock surfaces, moraines and sparse erratic boulders (Figure 3). The intensity of weathering processes in the Maritime Antarctic explains the absence of abundant and well-preserved glacial surfaces, which greatly constrained the rock sampling strategy. Following glacial retreat, frost shattering has affected the rock surface of both erosional (i.e., polished bedrock) and depositional (i.e., moraine and erratic boulders) glacial landforms. In addition, the frequent freeze–thaw cycles promote frost heaving, which together with nivation processes, enhances slow mass wasting dynamics in gentle to moderate hillsides, favouring the remobilisation of sediments from their original location. Therefore, caution was taken when collecting samples for CRE dating.

Field reconnaissance indicated an absence of glacial landforms on the higher surface of the northern plateau, and it was therefore eliminated as a candidate for CRE sampling. However, the lowlands surrounding its slopes include well-preserved glacial landforms (Figure 3):

a. *NW fringes of the plateau*. Small glacial cirques expand from the plateau edge to the NW limit of the peninsula towards the coast for more than 1.5 km. We observed two well-preserved polished bedrock surfaces close to the coast, at ca. 1 km from the cirque headwall—defined by the plateau edge—from where two samples were taken (ART-32, ART-33). At ca. 400 m from the cirque wall, we found a recessional moraine damming two small lakes that was intensely affected by post-glacial erosion, not favouring the preservation of boulders for CRE dating. Only one large and stable boulder cleaved by frost action was found in the northern part of this recessional moraine ridge, and therefore was sampled (ART-37). Upslope from this moraine, at ca. 250 m from the wall, polished bedrock was sampled (ART-38). At the foot of the plateau, there are two small cirques, which currently host small static glaciers or permanent ice patches. These cirques are enclosed by frontal moraines—one in the northern cirque and two in the southern one—at 100–150 m from the headwall. The moraine ridges located next to ice patches are still subject to the accumulation of debris

TABLE 4 AMS analytical data and calculated exposure ages. $^{36}Cl/^{35}Cl$ and $^{37}Cl/^{35}Cl$ ratios were inferred from measurements at the ASTER AMS facility. The numbers in brackets correspond to the internal (analytical) uncertainty at 1σ deviation.

Sample name	Sample weight (g)	Mass of Cl in spike[a] (mg)	$^{35}Cl/^{37}Cl$	$^{36}Cl/^{35}Cl$ (10^{-14})	[Cl] in sample (ppm)	[^{36}Cl] (10^4 atoms g^{-1})	Age (ka)
Southern N plateau							
ART-23	58.29	2.017	57.185 ± 1.756	3.644 ± 0.285	2.0	2.052 ± 0.191	6.1 ± 0.9 (0.7)
ART-24	65.27	2.017	49.355 ± 1.055	3.341 ± 0.302	2.2	1.682 ± 0.181	5.3 ± 0.8 (0.7)
ART-25	69.44	2.022	14.098 ± 0.416	5.841 ± 0.33	10.4	3.533 ± 0.238	7.0 ± 0.8 (0.7)
ART-26	72.38	2.020	16.714 ± 0.436	6.138 ± 0.365	7.9	3.406 ± 0.233	6.2 ± 0.7 (0.6)
ART-27	65.16	2.021	25.475 ± 0.677	5.298 ± 0.412	5.1	2.99 ± 0.259	6.8 ± 0.9 (0.8)
ART-28	71.12	2.013	29.992 ± 0.826	3.728 ± 0.306	3.8	1.826 ± 0.176	4.5 ± 0.7 (0.6)
Northern N plateau							
ART-32	73.97	1.981	18.139 ± 0.313	5.435 ± 0.451	6.8	2.818 ± 0.26	6.2 ± 0.9 (0.7)
ART-33	62.56	2.013	30.93 ± 0.664	5.577 ± 0.419	4.2	3.192 ± 0.266	8.1 ± 1.1 (0.9)
ART-34	69.44	2.015	15.158 ± 0.296	3.901 ± 0.417	9.4	2.243 ± 0.272	5.1 ± 0.8 (0.8)
ART-35	40.50	2.019	36.74 ± 1.237	1.999 ± 0.207	5.2	1.542 ± 0.218	4.6 ± 0.8 (0.7)
ART-36	66.83	2.014	28.924 ± 0.754	0.907 ± 0.133	4.2	0.334 ± 0.099	1.0 ± 0.3 (0.3)
ART-37	66.72	2.009	14.989 ± 0.798	3.698 ± 0.249	9.9	2.203 ± 0.184	6.3 ± 0.9 (0.8)
Blanks					**Total atoms Cl (10^{17})**	**Total atoms ^{36}Cl (10^4)**	–
BK-ART	–	2.010	218.848 ± 3.673	0.359 ± 0.12	1.735 ± 0.225	12.417 ± 4.158	–

[a]The ^{35}Cl carrier (spike) added to the samples was 261,018: [Cl] = 6.019 ± 0.115 mg Cl g^{-1}. $^{35}Cl/^{37}Cl$ ratio = 296.9 ± 3.6.

from the headwall, which slides down the snow surface and are therefore inappropriate for CRE dating. The outermost moraine ridge of the southern cirque is not affected by these processes, with very stable boulders that were sampled for CRE dating (ART-35, ART-36).

b. *S-SE slope of the plateau*. No features of glacial origin were found along the SW lowlands surrounding the plateau, but glacial features were identified at the S-SE margins of the plateau. At the foot of a small hollow where a small ice patch is located, we found polished surfaces showing traces of subglacial abrasion. These surfaces located at 50–70 m from the headwall were sampled for CRE dating (ART-23, ART-24). From this hollow, a small valley drains SE to a small bay (Figure 3). The area consists of heavily eroded volcanic and volcanoclastic gravels that form several staggered horizontal surfaces. Here, only four scattered large basalt boulders were found at 0.3–0.7 km from the headwall resting on the surface. They are interpreted as erratic boulders and were sampled for CRE dating (ART-25 to ART-28).

4.2 | Geochronological framework

The dataset including 12 CRE samples provides ages spanning from 8.1 ± 1.1 to 1.0 ± 0.3 ka (Table 4). Exposure ages are generally consistent with the spatial distribution and geomorphological setting of the dated surfaces (Figure 3).

Two samples collected from polished bedrock surfaces in the northern tip of the Fildes Peninsula reported CRE ages of 6.2 ± 0.9 ka (ART-32) and 8.1 ± 1.1 ka (ART-33), with a mean of 7.2 ± 1.7 ka (Figure 3). A similar average exposure age of 6.6 ± 0.9 ka was obtained from three erratic boulders distributed across the southern edge of the northern plateau: 7.0 ± 0.8 ka (ART-25), 6.2 ± 0.7 ka (ART-26) and 6.8 ± 0.9 ka (ART-25). A fourth sample that was dated at 4.5 ± 0.7 ka (ART-28) was identified as a potential outlier according to the chi-squared test (after Ward & Wilson, 1978) and therefore was excluded from the mean age calculation. At a slightly higher elevation, close to the plateau edge, two polished surfaces yielded exposure ages of 6.1 ± 0.9 ka (ART-23) and 5.3 ± 0.8 ka (ART-24), with a mean of 5.7 ± 1.0 ka (Figure 4).

The only boulder sampled from the external frontal moraine on the northern side of the peninsula resulted in an exposure age of 6.3 ± 0.9 ka (ART-37). In addition, a sample obtained from a polished bedrock surface in front of the frontal moraines yielded 5.1 ± 0.8 ka (ART-34), while two boulders from the moraine itself yielded two uneven exposure ages of 4.6 ± 0.8 ka (ART-35) and 1.0 ± 0.3 ka (ART-36), whose geomorphological meaning will be discussed.

5 | DISCUSSION

Geomorphological observations and the dataset of 12 ^{36}Cl CRE ages obtained from glacial records distributed across the northern sector of

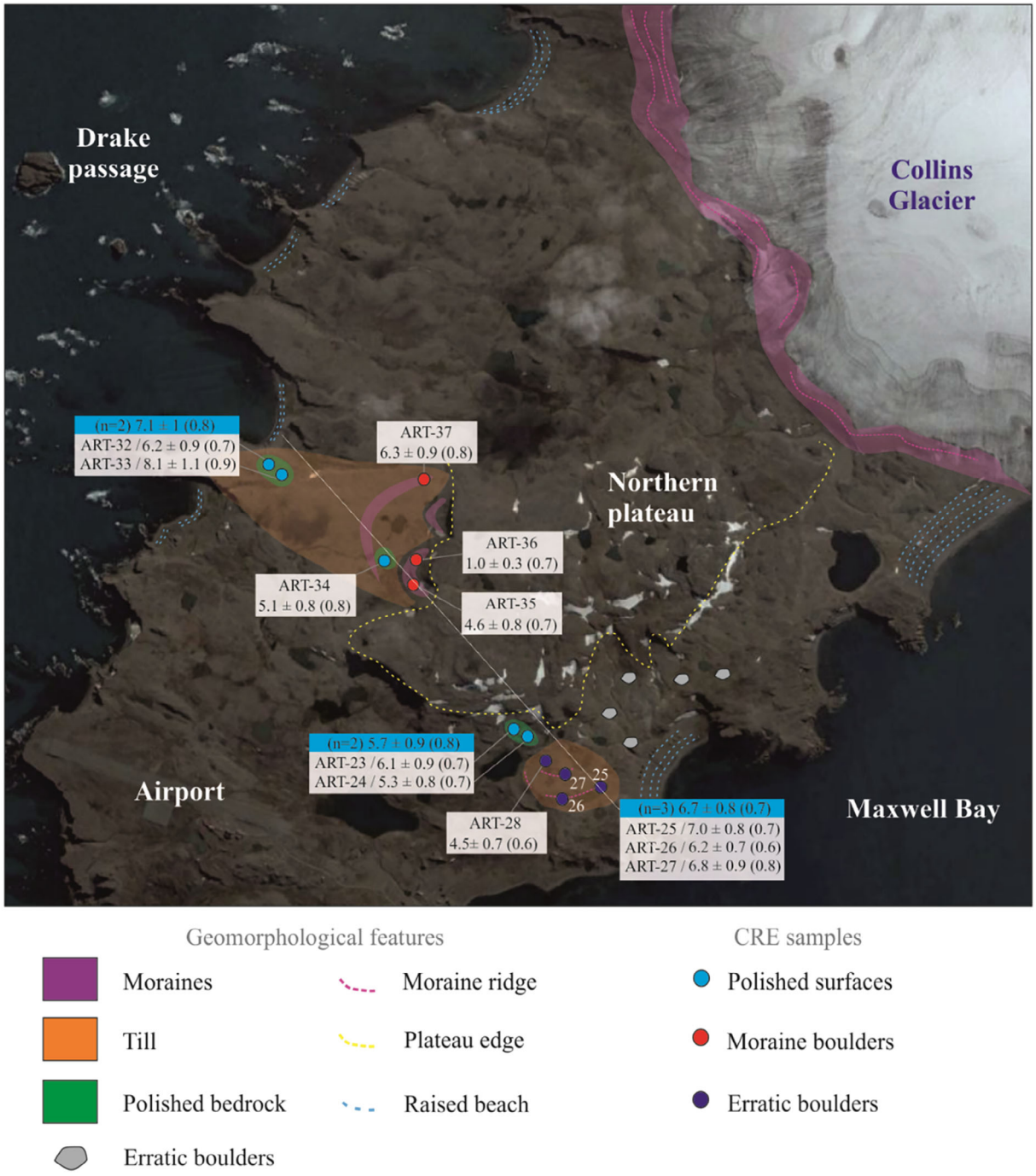

FIGURE 3 Geomorphological sketch of the northern plateau of the Fildes Peninsula (Satellite image source: Google Earth) including the main glacial features, as well as the CRE dates and the transect (line in white) shown in Figure 5. [Colour figure can be viewed at wileyonlinelibrary.com]

the Fildes Peninsula allowed reconstructing the spatio-temporal patterns of deglaciation during the Holocene.

5.1 | Holocene glacier oscillations in the northern Fildes Peninsula

The recent glacial retreat of Collins Glacier on the Fildes Peninsula must be framed within the long-term deglaciation that started following the LGM. Recent studies showed that the trend towards glacial retreat has accelerated over the last several decades, and suggested that the King George Ice Cap could disappear in less than three centuries if present-day glacial recession rates continue (Rückamp et al., 2011). A better understanding of the long-term glacier response is needed to assess whether present-day trends have already occurred in the geological record or represent the unprecedented effects in Antarctica of the current global warming.

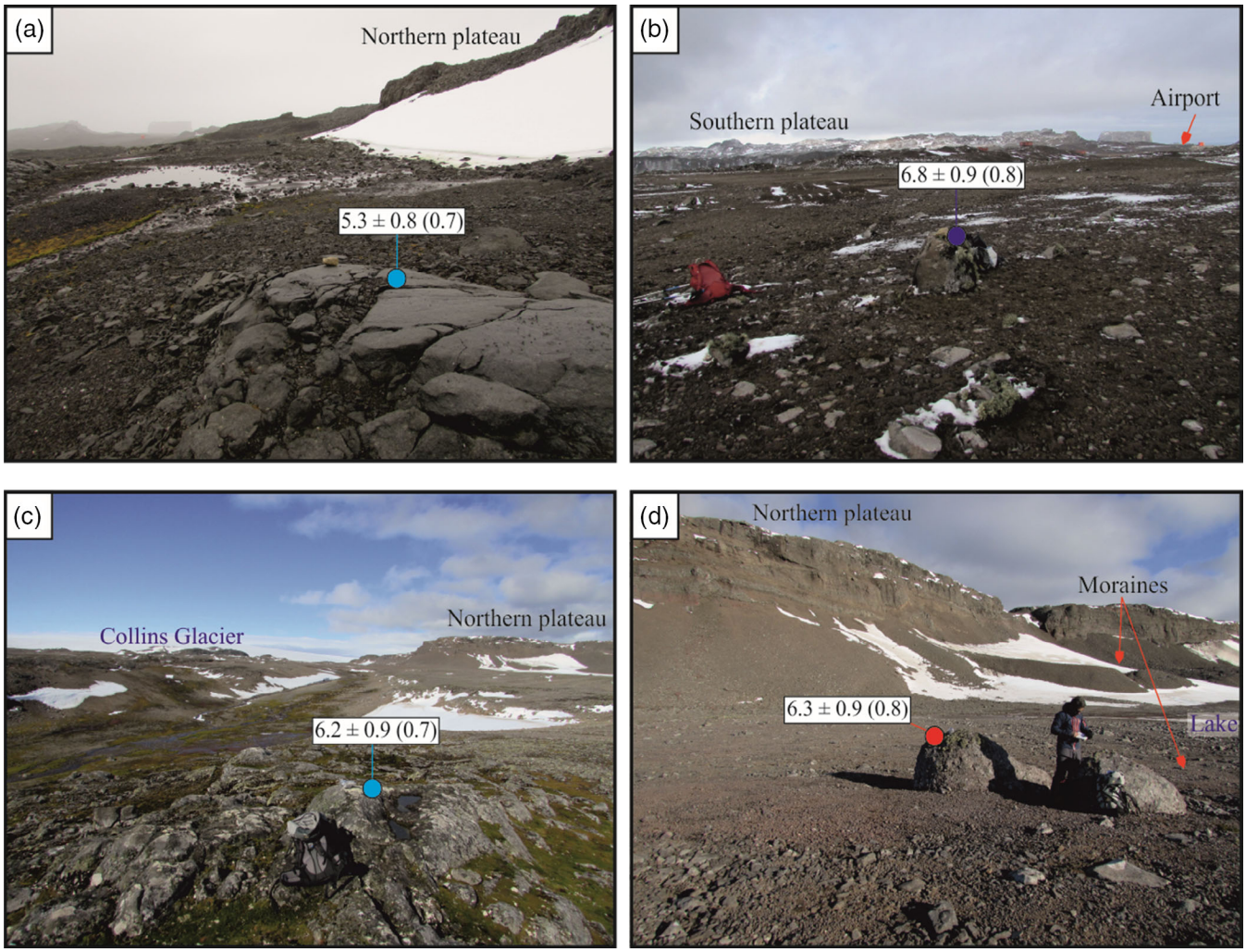

FIGURE 4 Examples of different glacial features and the corresponding CRE ages (ka). [Colour figure can be viewed at wileyonlinelibrary.com]

On the Fildes Peninsula, however, the absence of widespread well-preserved glacial records hinders the identification of post-LGM glacial oscillations. As in the rest of Maritime Antarctica, intense weathering processes following deglaciation are such that moraine systems formed over the last centuries to decades are heavily dismantled (Oliva & Ruiz-Fernández, 2015). This makes the reconstruction of the chronology of glacial retreats and culmination of advances using glacial records even more challenging and shows evidence of the need to combine multiple dating techniques and natural archives to infer the past environmental history in these areas.

Our CRE results suggest that the entire northern sector of the Fildes Peninsula must have become deglaciated at ca. 7 ka (Figure 5). The polished bedrock surfaces of the northern coast yielded a mean exposure age of 7.2 ± 1.7 ka, whereas the erratic boulders distributed at the foot of the southern edge of the northern plateau yielded 6.6 ± 0.9 ka. It is unlikely that the relatively flat northern plateau hosted ice at this time while the lowlands were mostly deglaciated: the low elevation difference (ca. 40–60 m) and the intense snow drifting must have impeded snow accumulation and its subsequent transformation into ice. In addition, basal sediments from Hochlandsee Lake confirm also that the NE corner of the northern plateau—closer to the Collins Glacier front (Figure 6)—was also deglaciated by, at least, 6.1 ka cal BP (Maüsbacher, 1991).

Geomorphic evidence across the S-SE edges of the plateau suggests that the deglaciation was not a continuous process. Scattered erratic boulders were present, in addition to glacially transported boulders and moraines that reflected periods of glacial readvance, stabilisation and retreat. This is also the case of the external moraine in the northern side of the peninsula, associated to a small local glacier flowing northwards towards the Drake Passage, where one boulder provided an exposure age of 6.3 ± 0.9 ka. Some of the erratic boulders on the S-SE rim of the plateau may also have been deposited during this phase. Subsequently, glacier recession must have prevailed between 5.7 ± 1.0 and 5.1 ± 0.8 ka as revealed by polished bedrock surfaces on the southern and northern sides of the plateau.

Geochronological and geomorphological evidence suggests that the deglaciation of the northern sector of the Fildes Peninsula resulted from the north-westerly Holocene retreat of the King George

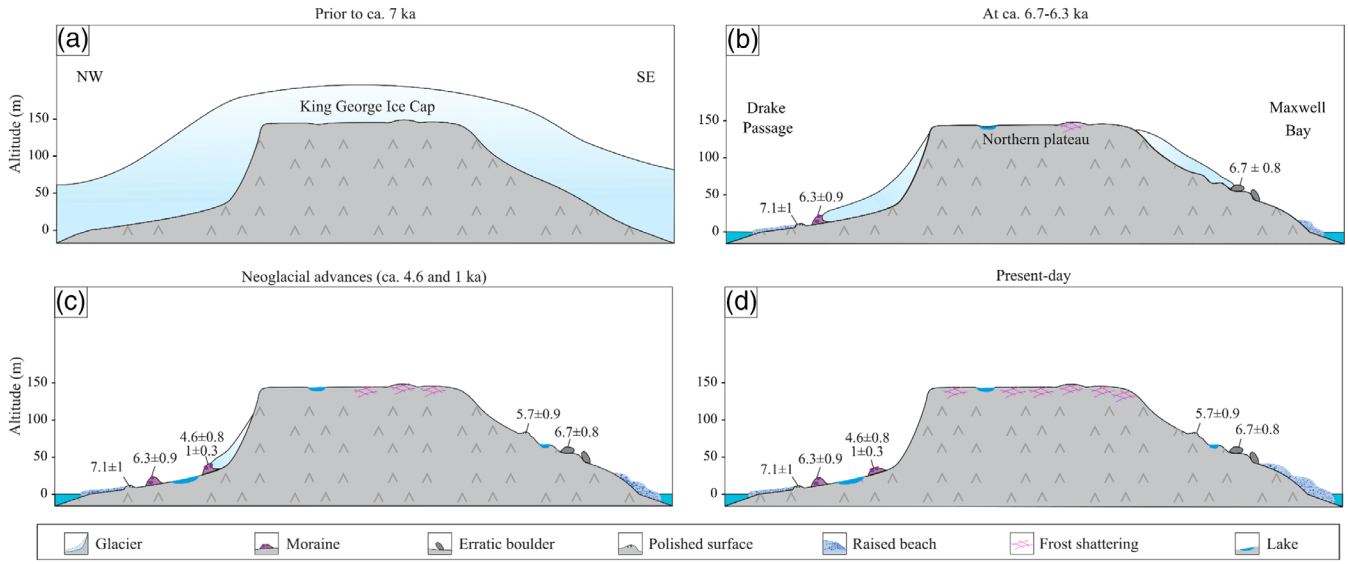

FIGURE 5 Tentative model of deglaciation based on our CRE ages: (a) The King George Ice Cap covers the entire peninsula; (b) Glaciers ca. 1 km long descend to the coastal margins forming moraines and dropping erratic boulders during retreat; (c) a small glacier developed on the leeward side of the northern peninsula fed by snow deflation processes; and (d) present-day situation with the area completely deglaciated. Note that frost shattering following glacial retreat has dismantled the exposed bedrock in the high terrain of the northern plateau, impeding the preservation of appropriate samples for CRE dating. [Colour figure can be viewed at wileyonlinelibrary.com]

Ice Cap, together with the gradual shrinkage of the small glaciers surrounding the plateau. The HTM must have favoured rapid deglaciation, particularly intense at 7–6 ka, when most of the northern sector of the Fildes Peninsula was exposed. However, during cold phases following the HTM, small glaciers may have formed in topographically sheltered areas at the foot of the plateau.

While the northern plateau's culminating surface was deglaciated and subjected to the effects of intense frost shattering processes, which eventually led to the disappearance of most of the glacial landforms, snow drifting allowed the survival of cirque glaciers sheltered by the slopes of the W-NW margin of the plateau that are enclosed by cirque moraines. The role of drifting snow in cirques surrounding plateaus has been already identified in Norway, where small changes in the prevailing climate conditions triggered changes in the elevation of the equilibrium line altitudes and favoured glacial advances or retreats (Dahl & Nesje, 1992). Today these cirques host small permanent ice patches that must have expanded during the last phases of deglaciation forming ca. 1-km-long ice tongues that generated moraines (Figure 3). After forming the outermost moraine, the small glaciers remained confined in the cirques. The maximum age of these moraines is constrained by the age of the outermost recessional moraine (6.3 ± 0.9 ka) and the age of the innermost polished outcrops (5.1 ± 0.8 ka), therefore they must be younger than 6–5 ka. The innermost part of these moraines was not dated, as it is still receiving debris supplied by the walls and descending through the ice and snow ramps. However, the two selected samples (ART-35 and 36) were located far away, defining the outermost moraine closing the cirque. Although their two exposure ages (4.6 ± 0.8 ka and 1.0 ± 0.3 ka) are not consistent with each other and it is impossible to determine if one of them represents the true timing of moraine deposition, they are both younger than the outer recessional moraine and the polished bedrocks that constrain them. They also fall within the Neoglacial period and thus agree with the stratigraphic sequence. These Neoglacial advances were of reduced scope, but they provide information about the glaciation pattern across the area. More intense, colder conditions must have favoured a larger expansion of these glacial spots surrounding the plateau, which likely merged with the westwards expansion of the Collins Glacier, covering the entire northern sector of the Fildes Peninsula. Our results support this multiple-glacier spot model instead of a single independent ice cap that expanded or retreated according to prevailing climate conditions. However, we are cautious in this interpretation given the limited number of ages from the moraine, although the small number of dates is somewhat compensated for by the overall coherence of the CRE data, and we suggest that more data are needed to confirm this hypothesis. In any event, the climatic significance of these ages may be of high interest for the region as they seem to suggest the occurrence of at least two phases of Neoglacial advance in the area.

Since then, glacial oscillations must have been restricted to the foreland of the Collins Glacier, where the different moraine ridges are indicative of phases of glacier advance and stabilisation for the last centuries (Petsch et al., 2020). The intensely remobilised sediments as well as the absence of vegetation also suggest a recent formation that Hall (2007) constrained at <0.65 ka cal BP. Indeed, the author also suggested that the maximum glacier advance over the last 3.5 ka cal BP has not exceeded <400–500 m beyond the present-day glacier.

In conclusion, glacial dynamics must have played a prominent role in the configuration of the present-day landscape but have also impacted environmental processes following the deglaciation of the area. In this sense, the variations of the ice volume stored in the SSI

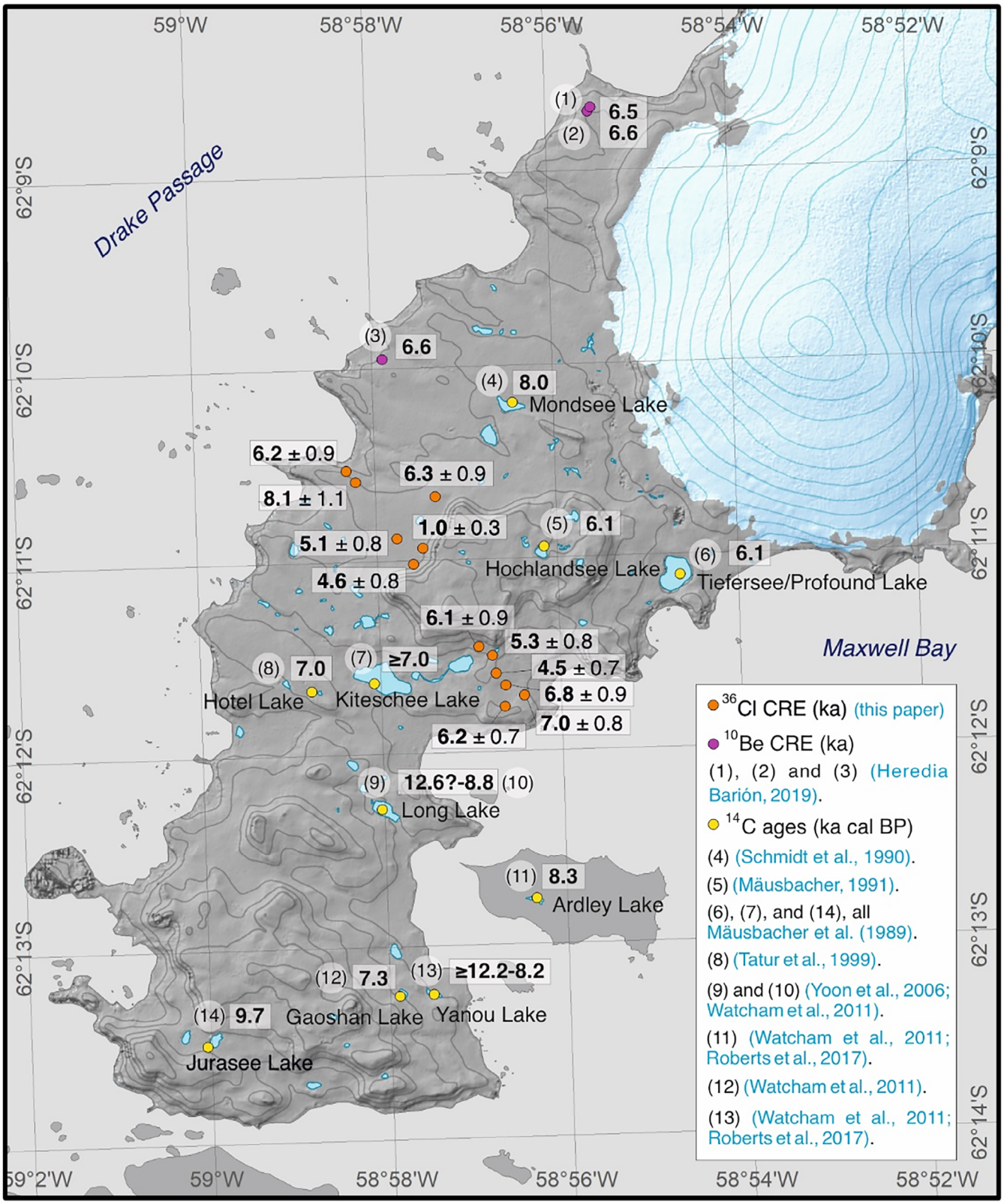

FIGURE 6 Distribution of existing radiocarbon ages and CRE results from the Fildes Peninsula (modified from Heredia Barión, 2019). [Colour figure can be viewed at wileyonlinelibrary.com]

during the Holocene have promoted the development of raised beaches in several coves alongside the Maxwell Bay at elevations between 2 and 21 m a.s.l. (Fretwell et al., 2010; Hall, 2010). In addition, the age of deglaciation is crucial to understand the spatial distribution of geomorphic processes that tend to show a higher activity between the northern plateau and the forelands of the Collins

Glacier than in areas of earlier deglaciation: surface runoff, active layer dynamics and periglacial activity (Michel, Schaefer, Simas, et al., 2014), the degree of soil development (Boy et al., 2016) or lacustrine sedimentation (Carrizo et al., 2019).

5.2 | New contributions to the deglaciation history of KGI and the SSI

The shrinkage of the King George Ice Cap since the LGM has promoted the exposure of several ice-free areas along the margins of the island as well as of several nunataks protruding the ice cap, particularly along its edges. During the LGM, the SSI were covered by an ice cap centred between Greenwich and Robert islands and connected with the AP ice sheet through the southern sector of the archipelago (Cofaigh et al., 2014). There is increasing evidence of ice thinning during the LGM at ca. 22 ka based on ^{10}Be ages at different elevations from several nunataks in Livingston Island, with a period of accelerated thinning between ca. 19.5 and 13 ka (^{10}Be Fernández-Fernández et al., 2021; M. Oliva et al., unpublished data). This pattern is also confirmed by ^{36}Cl exposure ages of the highest land surfaces above 250 m on Barton Penisula, KGI, which indicate the deglaciation of the highest peaks at ca. ~17.6 ka (Seong et al., 2009). Ice thinning was accompanied by extensive glacial retreat, with the appearance of many bays and fjords in the SSI archipelago. Climate amelioration also promoted the shrinkage of the ice shelf connecting the SSI with the AP ice sheet, which had started by 17.5 ka cal BP (Banfield & Anderson, 1995); in fact, by 10.1 ka cal BP the Bransfield Strait was mostly ice free (Simms, Milliken, et al., 2011).

At the onset of the Holocene, the major islands of the SSI were almost fully glaciated with independent ice caps covering the current ice-free environments (Ingólfsson et al., 1998). A period of rapid glacial retreat between 10.1 and 8.2 ka cal BP was detected in Maxwell Bay (Milliken et al., 2009), driven by warmer temperatures across the AP during the Early Holocene as revealed by ice and marine records as well as by geomorphological evidence (Bentley et al., 2009). As a result, low-altitude environments with relatively flat topography that were distally located from the accumulation areas of ice caps started to become ice free at this time. In the southern sector of the Fildes Peninsula, the basal sediments of several lakes showed evidence of ice-free conditions at 10–8 ka cal BP (Maüsbacher, 1991; Mäusbacher et al., 1989; Roberts et al., 2017; Schmidt et al., 1990; Tatur et al., 2004; Watcham et al., 2011; Yoon et al., 2006). Some of these studies also revealed that the deglaciation of the northern sector of the peninsula occurred between 8 and 6.1 ka (Figure 6). Our CRE ages agree well with the deglaciation of the northern sector of the Fildes Peninsula by 7–6 ka (Figure 5). This is also in agreement with CRE ages introduced by Heredia Barión (2019) who ^{10}Be-dated three polished surfaces in the lowlands of the northern plateau at 6.6–6.5 ka (Figure 6). Indeed, our results agree well with the reconstruction of Holocene isostatic rebound rates, which were at a maximum at 7.3–7 ka cal BP (Fretwell et al., 2010; Hall, 2010), a time when our results indicate that the northern plateau of the Fildes Peninsula was undergoing intense deglaciation.

The age of deglaciation of the northern sector of the Fildes Peninsula shows a very similar pattern to that observed at Byers Peninsula, the largest ice-free area in the SSI and an area from where further evidence of past environmental evolution is available. Here, lake sediment records revealed that the central plateau was deglaciated between 8.3 and 5.1 ka cal BP and that the ice cap has been relatively stable over the last two millennia, with the formation of a polygenic moraine (Oliva, Antoniades, Giralt, Granados, Pla-Rabes, Toro, Liu, et al., 2016; Oliva, Antoniades, Giralt, Granados, Pla-Rabes, Toro, & Sanjurjo, 2016; Toro et al., 2013). This peninsula is one of the few areas of the SSI where CRE has been directly applied to Holocene glacial records; results indicated the occurrence of two Neoglacial advances of the southern flank of the Rotch Dome Glacier as revealed by the clustering ^{36}Cl ages of the external line of erratic boulders (4.6 ± 0.8 ka) and one internal moraine ridge (1.0 ± 0.3 ka) near the edges of the ice cap (Palacios et al., 2020). The ages of two boulders from the same ridge on the Fildes Peninsula (4.6 ± 0.8 ka and 1.0 ± 0.3 ka) were very similar to those from Byers Peninsula.

The advances detected on the Fildes and Byers peninsulas at ca. 4.6–4.1 and 1.0 ka were of very reduced extent, given that the dated boulders and surfaces are actually very close to present-day glacial fronts. However, the chronology of Neoglacial oscillations on the Byers and Fildes peninsulas agrees well with other geomorphological evidence found across the AP, corroborating the existence of a Neoglacial phase after the HTM. In the context of the SSI, most authors considered the end of glacial retreat, and almost complete and definitive stabilisation of glacier margins, to have occurred at 5.5 ka (Barsch & Mäusbacher, 1986; Bentley et al., 2005; Björck et al., 1991; Björck et al., 1993; Björck et al., 1996; Hall, 2010; Maüsbacher, 1991; Mäusbacher et al., 1989; Oliva, Serrano, Gómez-Ortiz, González-Amuchastegui, Nieuwendam, Palacios, Pérez-Alberti, et al., 2016; Simms et al., 2012; Simms, DeWitt, et al., 2011; Toro et al., 2013; Valle et al., 2002; Watcham et al., 2011). Palaeoclimatic data, as well as the established regional glacial evolution, support the hypothesis that the small cirque moraines on the NW side of the northern Fildes plateau were generated during Neoglacial advances synchronous with others across the SSI. Indeed, there is widespread evidence from lake records, marine sediments and ice cores in the AP region, as well as the rest of the Antarctic continent, of significant cooling at 5 ka cal BP that favoured glacial advances (Barnard et al., 2014; Bentley et al., 2009; Carrivick et al., 2012; Cofaigh et al., 2014; Davies et al., 2012; Davies et al., 2017; Heroy et al., 2008; Kaplan et al., 2020; Khim et al., 2002; Michalchuk et al., 2009; Mosley-Thompson, 1996; Shevenell et al., 2011; Zale & Karlén, 1989). Similarly, there is evidence of a reintensification of cooling between 1.8 and 1.4 ka cal BP that led to glacial regrowth (Abram et al., 2013; Allen et al., 2010; Barnard et al., 2014; Bentley et al., 2009; Björck et al., 1996; Čejka et al., 2020; Davies et al., 2012; Davies et al., 2014; Domack et al., 2001; Heroy et al., 2008; Hodgson et al., 2013; Kaplan et al., 2020; Khim et al., 2002; Michalchuk et al., 2009; Mosley-Thompson, 1996; Mulvaney et al., 2012; Shevenell et al., 2011; Yoon et al., 2010). Moreover, the location of the glaciers, as well as glacial landforms on marine terraces dated after 5 ka, suggests that glaciers

in the SSI advanced following the HTM in some sectors (Everett, 1971; Hall, 2007; Hall, 2009), although this is not observed on the Fildes Peninsula.

6 | CONCLUSIONS

Glacial retreat plays a key role in the configuration of currently ice-free areas in Antarctica as it controls geomorphological and ecosystem dynamics in terrestrial environments. Understanding the chronology and pattern of glacial retreat is, therefore, crucial to understand present-day landscape dynamics and to frame recent observed trends within the context of natural responses of Antarctic ecosystems. The northern AP, long defined as one of the areas where recent warming has been most pronounced, includes large ice-free regions whose age of exposure is unknown. Although the Fildes Peninsula is among the regions of the continent with the greatest availability of chronological data, much information about spatio-temporal patterns of glacial oscillations since the last glacial cycle remains missing. Here, using CRE ages, we introduce the first chronology of glacial retreat focusing on the northern sector of the Fildes Peninsula.

Our results confirm that the deglaciation of the Fildes Peninsula was related not only to the dynamics of the King George Ice Cap, but was also dependent on smaller glaciers along the margins of the northern plateau, where snow accumulated in the lee side of the plateau. New ^{36}Cl CRE ages show evidence that the northern plateau's major deglaciation occurred during the HTM. Glacial retreat was rapid at ca. 7–6 ka in response to prevailing warm conditions, and the entire area was probably ice free by ca. 6 ka. Subsequently, as temperatures decreased during the Neoglacial, small glaciers were most likely formed in the small but steep cirques of the plateau's northern edges. The moraines, which close the cirques, show evidence of the possible occurrence of several periods during the last millennia with favourable climate conditions for aggrading sediments on these polygenic moraines, particularly at ca. 4.6 and 1 ka. These results are very similar to those observed in other ice-free environments in the SSI, such as the Byers Peninsula, where the major deglaciation of the plateau also occurred during the HTM, and two Neoglacial advances were detected at ca. 4 and 1 ka. Other records such as lacustrine sediments and raised beaches also confirm these major phases of glacial retreat and advance during the Holocene in the SSI and in the AP.

This research constitutes a step forward in our understanding of Holocene glacier fluctuations in Antarctica. However, further research needs to be conducted to expand the number of areas from where such paleoenvironmental information is available, to integrate marine versus terrestrial records and to provide further chronological control for some phases crucial to framing recent trends, such as the timing and magnitude of climate and glacial response during the LIA. Future work should focus on the CRE dating of the current frontal moraine system to elucidate the timing of recent advances in the Collins Glacier.

ACKNOWLEDGEMENTS

This research was funded by the NUNANTAR (Fundação para a Ciência e Tecnologia of Portugal; 02/SAICT/2017 – 32002) and CRONOANTAR (Ministerio de Economía y Competitividad, Spain, CTM2016-77878-P) projects. Field research was also supported by the research groups ANTALP (Antarctic, Arctic, Alpine Environments; 2017-SGR-1102) funded by the Agència de Gestió d'Ajuts Universitaris i de Recerca of the Government of Catalonia as well as by the ZEPHYRUS (Climate Change and Environmental Systems) and College on Polar and Extreme Environments (Polar2E) of the Universidade de Lisboa. The study topics complement those of the project NEOGREEN (PID2020-113798GB-C31) funded by the Spanish Ministerio de Economía y Competitividad. Marc Oliva is supported by the Ramón y Cajal Program (RYC-2015-17597) and Marcelo Fernandes by a PhD fellowship of the Fundação para a Ciência e Tecnologia of Portugal (UIDB/00295/2020). The ^{36}Cl measurements were performed at the ASTER AMS national facility (CEREGE, Aix-en-Provence), which is supported by the INSU/CNRS and the ANR through the "Projets thématiques d'excellence" program for the "Equipements d'excellence" ASTER-CEREGE action and IRD. We are also grateful to Artigas Station for their support during the field work season.

CONFLICT OF INTEREST STATEMENT

All authors declare that they have no conflicts of interest.

DATA AVAILABILITY STATEMENT

The data that support the findings of this study are available from the corresponding author upon reasonable request.

ORCID

Marc Oliva https://orcid.org/0000-0001-6521-6388

José M. Fernández-Fernández https://orcid.org/0000-0002-6948-1530

REFERENCES

Abram, N. J., Mulvaney, R., Wolff, E. W., Triest, J., Kipfstuhl, S., Trusel, L. D., Vimeux, F., Fleet, L., & Arrowsmith, C. (2013). Acceleration of snow melt in an Antarctic peninsula ice core during the twentieth century. *Nature Geoscience*, *6*, 404–411. https://doi.org/10.1038/ngeo1787

Allen, C. S., Oakes-Fretwell, L., Anderson, J. B., & Hodgson, D. A. (2010). A record of Holocene glacial and oceanographic variability in Neny Fjord, Antarctic peninsula. *Holocene*, *20*, 551–564. https://doi.org/10.1177/0959683609356581

ATCM. (2009). Management plan for Antarctic specially protected area No.125 – Fildes peninsula. King George Island.

Banfield, L. A., & Anderson, J. B. (1995). Seismic Facies investigation of the late Quarternary glacial history of Bransfield Basin, Antarctica. In *Geology and seismic stratigraphy of the Antarctic margin, Antarctic research series* (pp. 123–140). American Geophysical Union. https://doi.org/10.1029/AR068p0123

Barnard, A., Wellner, J. S., & Anderson, J. B. (2014). Late Holocene climate change recorded in proxy records from a Bransfield Basin sediment core, Antarctic Peninsula. *Polar Research*, *33*, 1–13. https://doi.org/10.3402/polar.v33.17236

Barsch, D., & Mäusbacher, R. (1986). New data on the relief development of the South Shetland Islands, Antarctica. *Interdisciplinary Science Reviews*, *11*, 211–218. https://doi.org/10.1179/isr.1986.11.2.211

Bentley, M. J., Hodgson, D. A., Smith, J. A., Cofaigh, C. Ó., Domack, E. W., Larter, R. D., Roberts, S. J., Brachfeld, S., Leventer, A., Hjort, C.,

Hillenbrand, C. D., & Evans, J. (2009). Mechanisms of Holocene palaeoenvironmental change in the Antarctic peninsula region. *Holocene*, *19*, 51–69. https://doi.org/10.1177/0959683608096603

Bentley, M. J., Hodgson, D. A., Smith, J. A., & Cox, N. J. (2005). Relative Sea level curves for the South Shetland Islands and Marguerite Bay, Antarctic peninsula. *Quaternary Science Reviews*, *24*, 1203–1216. https://doi.org/10.1016/j.quascirev.2004.10.004

Björck, S., Hakansson, H., Olsson, S., Barnekow, L., & Janssens, J. (1993). Palaeoclimatic studies in South Shetland Islands, Antarctica, based on numerous stratigraphic variables in lake sediments. *Journal of Paleolimnology*, *8*, 233–272. https://doi.org/10.1007/BF00177858

Björck, S., Håkansson, H., Zale, R., Karlén, W., & Jönsson, B. L. (1991). A late Holocene lake sediment sequence from Livingston Island, South Shetland Islands, with palaeoclimatic implications. *Antarctic Science*, *3*, 61–72. https://doi.org/10.1017/S095410209100010X

Björck, S., Olsson, S., Ellis-Evans, C., Håkansson, H., Humlum, O., & de Lirio, J. M. (1996). Late Holocene palaeoclimatic records from lake sediments on James Ross Island, Antarctica. *Palaeogeography, Palaeoclimatology, Palaeoecology*, *121*, 195–220. https://doi.org/10.1016/0031-0182(95)00086-0

Bockheim, J., Vieira, G., Ramos, M., López-Martínez, J., Serrano, E., Guglielmin, M., Wilhelm, K., & Nieuwendam, A. (2013). Climate warming and permafrost dynamics in the AP region. *Global and Planetary Change*, *100*, 215–223. https://doi.org/10.1016/j.gloplacha.2012.10.018

Boy, J., Godoy, R., Shibistova, O., Boy, D., McCulloch, R., De La Fuente, A. A., Morales, M. A., Mikutta, R., & Guggenberger, G. (2016). Successional patterns along soil development gradients formed by glacier retreat in the maritime Antarctic, King George Island. *Revista Chilena de Historia Natural*, *89*, 1–17. https://doi.org/10.1186/s40693-016-0056-8

Briner, J. P., Cuzzone, J. K., Badgeley, J. S., Young, N. E., Steig, E. J., Morlighem, M., Schlegel, N.-J., Hakim, G. J., Schaefer, J., Johnson, J. V., Lesnek, A. J., Thomas, E. K., Allan, E., Bennike, O., Cluett, A. A., Csatho, B., de Vernal, A., Downs, J., Larour, E., & Nowicki, S. (2020). Greenland ice sheet mass loss rate will exceed Holocene values this century. *Nature*, *586*, 70–74. https://doi.org/10.1038/s41586-020-2742-6

Burton-Johnson, A., Black, M., Peter, T. F., & Kaluza-Gilbert, J. (2016). An automated methodology for differentiating rock from snow, clouds and sea in Antarctica from Landsat 8 imagery: A new rock outcrop map and area estimation for the entire Antarctic continent. *The Cryosphere*, *10*, 1665–1677. https://doi.org/10.5194/tc-10-1665-2016

Carrivick, J. L., Davies, B. J., Glasser, N. F., Nývlt, D., & Hambrey, M. J. (2012). Late-Holocene changes in character and behaviour of land-terminating glaciers on James Ross Island, Antarctica. *Journal of Glaciology*, *58*, 1176–1190. https://doi.org/10.3189/2012JoG11J148

Carrizo, D., Sánchez-García, L., Menes, R. J., & García-Rodríguez, F. (2019). Discriminating sources and preservation of organic matter in surface sediments from five Antarctic lakes in the Fildes peninsula (King George Island) by lipid biomarkers and compound-specific isotopic analysis. *Science of the Total Environment*, *672*, 657–668. https://doi.org/10.1016/j.scitotenv.2019.03.459

Čejka, T., Nývlt, D., Kopalová, K., Bulínová, M., Kavan, J., Lirio, J. M., Coria, S. H., & van de Vijver, B. (2020). Timing of the neoglacial onset on the north-eastern Antarctic peninsula based on lacustrine archive from Lake Anónima, Vega Island. *Global and Planetary Change*, *184*, 103050. https://doi.org/10.1016/j.gloplacha.2019.103050

Clark, P., Dyke, A., Shakun, J., Carlson, A., Clark, J., Wohlfarth, B., Mitrovica, J., Hostetler, S., & McCabe, A. (2009). The last glacial maximum. *Science*, *325*, 710–714. https://doi.org/10.1126/science.1172873

Cofaigh, Ó., C., Davies, B. J., Livingstone, S. J., Smith, J. A., Johnson, J. S., Hocking, E. P., Hodgson, D. A., Anderson, J. B., Bentley, M. J., Canals, M., Domack, E., Dowdeswell, J. A., Evans, J., Glasser, N. F., Hillenbrand, C.-D. D., Larter, R. D., Roberts, S. J., Simms, A. R., … Simms, A. R. (2014). Reconstruction of ice-sheet changes in the AP since the last glacial maximum. *Quaternary Science Reviews*, *100*, 87–110. https://doi.org/10.1016/j.quascirev.2014.06.023

Convey, P., Biersma, E. M., Casanova-Katny, A., & Maturana, C. S. (2020). Refuges of Antarctic diversity. In M. Oliva & J. Ruiz-Fernández (Eds.), *Past Antarctica* (pp. 181–200). Elsevier.

Dahl, S. O., & Nesje, A. (1992). Paleoclimatic implications based on equilibrium-line altitude depressions of reconstructed younger Dryas and Holocene cirque glaciers in inner Nordfjord, western Norway. *Palaeogeography Palaeoclimatology Palaeoecology*, *94*, 87–97. https://doi.org/10.1016/0031-0182(92)90114-K

Davies, B. J., Golledge, N. R., Glasser, N. F., Carrivick, J. L., Ligtenberg, S. R. M., Barrand, N. E., Van Den Broeke, M. R., Hambrey, M. J., & Smellie, J. L. (2014). Modelled glacier response to centennial temperature and precipitation trends on the Antarctic peninsula. *Nature Climate Change*, *4*, 993–998. https://doi.org/10.1038/nclimate2369

Davies, B. J., Hambrey, M. J., Glasser, N. F., Holt, T., Rodés, A., Smellie, J. L., Carrivick, J. L., & Blockley, S. P. E. (2017). Ice-dammed lateral lake and epishelf lake insights into Holocene dynamics of Marguerite trough ice stream and George VI ice shelf, Alexander Island, Antarctic peninsula. *Quaternary Science Reviews*, *177*, 189–219. https://doi.org/10.1016/j.quascirev.2017.10.016

Davies, B. J., Hambrey, M. J., Smellie, J. L., Carrivick, J. L., & Glasser, N. F. (2012). Antarctic peninsula ice sheet evolution during the Cenozoic era. *Quaternary Science Reviews*, *31*, 30–66. https://doi.org/10.1016/j.quascirev.2011.10.012

Domack, E., Leventer, A., Dunbar, R., Taylor, F., Brachfeld, S., & Sjunneskog, C. (2001). Chronology of the palmer deep site, Antarctic peninsula: A Holocene palaeoenvironmental reference for the circum-Antarctic. *Holocene*, *11*, 1–9. https://doi.org/10.1191/095968301673881493

Dunai, T. (2010). *Cosmogenic nuclides, principles, concepts and applications in the earth surface sciences*. Cambridge University Press.

Dunne, J., Elmore, D., & Muzikar, P. (1999). Scaling factors for the rates of production of cosmogenic nuclides for geometric shielding and attenuation at depth on sloped surfaces. *Geomorphology*, *27*, 3–11. https://doi.org/10.1016/S0169-555X(98)00086-5

Everett, K. R. (1971). Observations on the glacial history of Livingston Island. *Arctic*, *24*, 41–50. https://doi.org/10.14430/arctic3111

Fernández-Fernández, J. M., Oliva, M., Palacios, D., Garcia-Oteyza, J., Navarro, F. J., Schimmelpfennig, I., Léanni, L., & Team, A. (2021). Ice thinning on nunataks during the glacial to interglacial transition in the AP region according to cosmic-ray exposure dating: Evidence and uncertainties. *Quaternary Science Reviews*, *264*, 107029. https://doi.org/10.1016/j.quascirev.2021.107029

Fink, D., Vogt, S., & Hotchkis, M. (2000). Cross-sections for 36Cl from Ti at ep=35–150 MeV: Applications to in-situ exposure dating. *Nuclear Instruments and Methods in Physics Research Section B: Beam Interactions with Materials and Atoms*, *172*, 861–866. https://doi.org/10.1016/S0168-583X(00)00200-7

Fretwell, P. T., Hodgson, D. A., Watcham, E. P., Bentley, M. J., & Roberts, S. J. (2010). Holocene isostatic uplift of the South Shetland Islands, AP, modelled from raised beaches. *Quaternary Science Reviews*, *29*, 1880–1893. https://doi.org/10.1016/j.quascirev.2010.04.006

Giralt, S., Hernández, A., Pla-Rabés, S., Antoniades, D., Toro, M., Granados, I., & Oliva, M. (2020). Holocene environmental changes deduced from lake sediments. In M. Oliva & J. Ruiz-Fernández (Eds.), *Past Antarctica* (pp. 51–68). Elsevier.

Gonzalez, S., & Vasallo, F. (2020). Antarctic Climates. In M. I. Goldstein & D. A. Della Sala (Eds.), *Encyclopedia of the World's biomes* (pp. 595–605). Elsevier.

Hall, B. L. (2007). Late-Holocene advance of the Collins ice cap, King George Island, South Shetland Islands. *The Holocene*, *17*, 1253–1258. https://doi.org/10.1177/0959683607085132

Hall, B. L. (2009). Holocene glacial history of Antarctica and the sub-Antarctic islands. *Quaternary Science Reviews*, *28*, 2213–2230. https://doi.org/10.1016/j.quascirev.2009.06.011

Hall, B. L. (2010). Holocene relative sea-level changes and ice fluctuations in the South Shetland Islands. *Global and Planetary Change*, *74*, 15–26. https://doi.org/10.1016/j.gloplacha.2010.07.007

Henriques, D. K., Silva, B. G. C., Zuñiga, G. E., & Câmara, P. E. A. S. (2018). Contributions to the bryological knowledge of ASPA 125, Fildes peninsula, King George Island. *Biological Research*, *51*, 1–7. https://doi.org/10.1186/s40659-018-0178-3

Heredia Barión, P. A. (2019). *Paleoenvironmental evolution of on-shore ice-free areas around Maxwell Bay, King George Island, South Shetland Islands*. Universität Bremen PhD thesis.

Heroy, D. C., Sjunneskog, C., & Anderson, J. B. (2008). Holocene climate change in the Bransfield Basin, Antarctic peninsula: Evidence from sediment and diatom analysis. *Antarctic Science*, *20*, 69–87. https://doi.org/10.1017/S0954102007000788

Hodgson, D. A., Roberts, S. J., Smith, J. A., Verleyen, E., Sterken, M., Labarque, M., Sabbe, K., Vyverman, W., Allen, C. S., Leng, M. J., & Bryant, C. (2013). Late quaternary environmental changes in Marguerite Bay, Antarctic peninsula, inferred from lake sediments and raised beaches. *Quaternary Science Reviews*, *68*, 216–236. https://doi.org/10.1016/j.quascirev.2013.02.002

Ingólfsson, Ó., Hjort, C., Berkman, P. A., Björck, S., Colhoun, E., Goodwin, I. D., Hall, B., Hirakawa, K., Melles, M., Möller, P., & Prentice, M. L. (1998). Antarctic glacial history since the last glacial maximum: An overview of the record on land. *Antarctic Science*, *10*, 326–344. https://doi.org/10.1017/S095410209800039X

Ivy-Ochs, S., Synal, H. A., Roth, C., & Schaller, M. (2004). Initial results from isotope dilution for Cl and 36Cl measurements at the PSI/ETH Zurich AMS facility. *Nuclear Instruments and Methods in Physics Research Section B: Beam Interactions with Materials and Atoms*, *223–224*, 623–627. https://doi.org/10.1016/j.nimb.2004.04.115

Kaplan, M. R., Strelin, J. A., Schaefer, J. M., Peltier, C., Martini, M. A., Flores, E., Winckler, G., & Schwartz, R. (2020). Holocene glacier behavior around the northern Antarctic peninsula and possible causes. *Earth and Planetary Science Letters*, *534*, 116077. https://doi.org/10.1016/j.epsl.2020.116077

Khim, B. K., Yoon, H. I., Kang, C. Y., & Bahk, J. J. (2002). Unstable climate oscillations during the late Holocene in the eastern Bransfield Basin, Antarctic peninsula. *Quaternary Research*, *58*, 234–245. https://doi.org/10.1006/qres.2002.2371

Li, Y. (2018). Determining topographic shielding from digital elevation models for cosmogenic nuclide analysis: A GIS model for discrete sample sites. *Journal of Mountain Science*, *15*, 939–947. https://doi.org/10.1007/s11629-018-4895-4

Lifton, N., Sato, T., & Dunai, T. J. (2014). Scaling in situ cosmogenic nuclide production rates using analytical approximations to atmospheric cosmic-ray fluxes. *Earth and Planetary Science Letters*, *386*, 149–160. https://doi.org/10.1016/J.EPSL.2013.10.052

López-Martínez, J., Serrano, E., Schmid, T., Mink, S., & Linés, C. (2012). Periglacial processes and landforms in the South Shetland Islands (northern AP region). *Geomorphology*, *155–156*, 62–79. https://doi.org/10.1016/j.geomorph.2011.12.018

Machado, A., Lima, E. F., Chemale, F., Morata, D., Oteiza, O., Almeida, D. P. M., Figueiredo, A. M. G., Alexandre, F. M., & Urrutia, J. L. (2005). Geochemistry constraints of Mesozoic-Cenozoic calc-alkaline magmatism in the south Shetland arc, Antarctica. *Journal of South American Earth Sciences*, *18*, 407–425. https://doi.org/10.1016/j.jsames.2004.11.011

Marrero, S. M., Phillips, F. M., Caffee, M. W., & Gosse, J. C. (2016). CRONUS-earth cosmogenic36Cl calibration. *Quaternary Geochronology*, *31*, 199–219. https://doi.org/10.1016/j.quageo.2015.10.002

Maüsbacher, R. (1991). *Die jungquartare Relief- und Klimageschichte im Bereich der Fildeshalbinsel Süd-Shetland Inseln*. Universität Heidelberg Geographisches Institut.

Mäusbacher, R., Müller, J., & Schmidt, R. (1989). Evolution of postglacial sedimentation in Antarctic lakes (King George Island). *Zeitschrift für Geomorphologie*, *33*, 219–234. https://doi.org/10.1127/zfg/33/1989/219

Merchel, S., Bremser, W., Alfimov, V., Arnold, M., Aumaître, G., Benedetti, L., Bourlès, D. L., Caffee, M., Fifield, L. K., Finkel, R. C., Freeman, S. P. H. T., Martschini, M., Matsushi, Y., Rood, D. H., Sasa, K., Steier, P., Takahashi, T., Tamari, M., Tims, S. G., … Xu, S. (2011). Ultra-trace analysis of 36Cl by accelerator mass spectrometry: An interlaboratory study. *Analytical and Bioanalytical Chemistry*, *400*, 3125–3132. https://doi.org/10.1007/s00216-011-4979-2

Michalchuk, B. R., Anderson, J. B., Wellner, J. S., Manley, P. L., Majewski, W., & Bohaty, S. (2009). Holocene climate and glacial history of the northeastern Antarctic peninsula: The marine sedimentary record from a long SHALDRIL core. *Quaternary Science Reviews*, *28*, 3049–3065. https://doi.org/10.1016/j.quascirev.2009.08.012

Michel, R., Schaefer, C., López-Martínez, J., Simas, F., Haus, N., Serrano, E., & Bockheim, J. G. (2014). Soils and landforms from Fildes peninsula and Ardley Island, maritime Antarctica. *Geomorphology*, *225*, 76–86. https://doi.org/10.1016/j.geomorph.2014.03.041

Michel, R. F. M., Schaefer, C. E. G. R., Simas, F. M. B., Francelino, M. R., Fernandes-Filho, E. I., Lyra, G. B., & Bockheim, J. G. (2014). Active-layer thermal monitoring on the Fildes peninsula, King George Island, maritime Antarctica. *Solid Earth*, *5*, 1361–1374. https://doi.org/10.5194/se-5-1361-2014

Milliken, K. T., Anderson, J. B., Wellner, J. S., Bohaty, S. M., Manley, P. L., Bay, M., & This, S. I. (2009). High-resolution Holocene climate record from Maxwell Bay, South Shetland Islands, Antarctica. *Bulletin of the Geological Society of America*, *121*, 1711–1725. https://doi.org/10.1130/B26478.1

Mosley-Thompson, E. (1996). *Holocene climate changes recorded in an East Antarctica ice Core*. NATO ASI Series (Vol. I41, pp. 263–279). Springer-Verlag Berlin Heidelberg.

Mulvaney, R., Abram, N., Hindmarsh, R. C. A., Arrowsmith, C., Fleet, L., Triest, J., Sime, L. C., Alemany, O., & Foord, S. (2012). Recent Antarctic peninsula warming relative to Holocene climate and ice-shelf history. *Nature*, *489*, 141–144. https://doi.org/10.1038/nature11391

Noble, T. L., Rohling, E. J., Aitken, A. R. A., Bostock, H. C., Chase, Z., Gomez, N., Jong, L. M., King, M. A., Mackintosh, A. N., McCormack, F. S., McKay, R. M., Menviel, L., Phipps, S. J., Weber, M. E., Fogwill, C. J., Gayen, B., Golledge, N. R., Gwyther, D. E., Hogg, A. M. C., … Williams, T. (2020). The sensitivity of the Antarctic ice sheet to a changing climate: Past, present, and future. *Reviews of Geophysics*, *58*, 1–89. https://doi.org/10.1029/2019RG000663

Nývlt, D., Glasser, N. F., Oliva, M., Roberts, S. J., & Roman, M. (2020). Tracing the deglaciation since the last glacial maximum. In M. Oliva & J. Ruiz-Fernández (Eds.), *Past Antarctica* (pp. 89–108). Elsevier.

Oliva, M., Antoniades, D., Giralt, S., Granados, I., Pla-Rabes, S., Toro, M., Liu, E. J., Sanjurjo, J., & Vieira, G. (2016). The Holocene deglaciation of the byers peninsula (Livingston Island, Antarctica) based on the dating of lake sedimentary records. *Geomorphology*, *261*, 89–102. https://doi.org/10.1016/j.geomorph.2016.02.029

Oliva, M., Antoniades, D., Giralt, S., Granados, I., Pla-Rabes, S., Toro, M., & Sanjurjo, J. (2016). La deglaciación de las áreas libres de hielo de las islas Shetland del Sur (Antártida): Ejemplos de Byers (Livingston) y Barton (King George). *Cuaternario y Geomorfologia*, *30*, 105–118. https://doi.org/10.17735/cyg.v30i1-2.48665

Oliva, M., Antoniades, D., Serrano, E., Giralt, S., Liu, E. J., Granados, I., Pla-rabes, S., Toro, M., & Hong, S. G. (2019). The deglaciation of Barton peninsula (King George Island, South Shetland Islands, Antarctica) based on geomorphological evidence and lacustrine records.

Oliva, M., & Ruiz-Fernández, J. (2015). Coupling patterns between Paraglacial and permafrost degradation responses in Antarctica. *Earth Surface Processes and Landforms*, *40*, 1227–1238. https://doi.org/10.1002/esp.3716

Oliva, M., & Ruiz-Fernández, J. (2017). Geomorphological processes and frozen ground conditions in elephant point (Livingston Island, South Shetland Islands, Antarctica). *Geomorphology*, *293*, 368–379. https://doi.org/10.1016/j.geomorph.2016.01.020

Oliva, M., Serrano, E., Gómez-Ortiz, A., González-Amuchastegui, M. J., Nieuwendam, A., Palacios, D., Pérez-Alberti, A., Pellitero, R., Ruiz-Fernández, J., Valcárcel, M., Vieira, G., & Antoniades, D. (2016). Spatial and temporal variability of periglaciation of the Iberian Peninsula. *Quaternary Science Reviews*, *137*, 176–199. https://doi.org/10.1016/j.quascirev.2016.02.017

Palacios, D., Ruiz-Fernández, J., Oliva, M., Andrés, N., Fernández-Fernández, J. M., Schimmelpfennig, I., Leanni, L., & González-Díaz, B. (2020). Timing of formation of neoglacial landforms in the South Shetland Islands (*Antarctic peninsula*): Regional and global implications. *Quaternary Science Reviews*, *234*, 106248. https://doi.org/10.1016/j.quascirev.2020.106248

Pasik, M., Bakuła, K., Różycki, S., Ostrowski, W., Kowalska, M. E., Fijałkowska, A., Rajner, M., Łapiński, S., Sobota, I., Kejna, M., & Osińska-Skotak, K. (2021). Glacier geometry changes in the western shore of admiralty bay, king George Island over the last decades. *Sensors*, *21*, 1–25. https://doi.org/10.3390/s21041532

Petsch, C., da Rosa, K. K., Vieira, R., Braun, M. H., Costa, R. M., & Simões, J. C. (2020). The effects of climatic change on glacial, proglacial and paraglacial systems at Collins glacier, King George Island, Antarctica, from the end of the little ice age to the 21st century. *Investigaciones Geograficas*. https://doi.org/10.14350/RIG.60153

Renssen, H., Seppä, H., Crosta, X., Goosse, H., & Roche, D. M. (2012). Global characterization of the Holocene thermal maximum. *Quaternary Science Reviews*, *48*, 7–19. https://doi.org/10.1016/j.quascirev.2012.05.022

Renssen, H., Seppä, H., Heiri, O., Roche, D. M., Goosse, H., & Fichefet, T. (2009). The spatial and temporal complexity of the holocene thermal maximum. *Nature Geoscience*, *2*, 411–414. https://doi.org/10.1038/ngeo513

RGI Consortium. (2017). Randolph glacier inventory – A dataset of global glacier outlines: Version 6.0: Technical report, global land ice measurements from space, Colorado, USA. Digital Media. https://doi.org/10.7265/N5-RGI-60

Roberts, S. J., Monien, P., Foster, L. C., Loftfield, J., Hocking, E. P., Schnetger, B., Pearson, E. J., Juggins, S., Fretwell, P., Ireland, L., Ochyra, R., Haworth, A. R., Allen, C. S., Moreton, S. G., Davies, S. J., Bentley, M. J., & Hodgson, D. A. (2017). Past penguin colony responses to explosive volcanism on the Antarctic peninsula. *Nature Communications*, *8*, 14914. https://doi.org/10.1038/ncomms14914

Rückamp, M., Braun, M., Suckro, S., & Blindow, N. (2011). Observed glacial changes on the King George Island ice cap, Antarctica, in the last decade. *Global and Planetary Change*, *79*, 99–109. https://doi.org/10.1016/j.gloplacha.2011.06.009

Ruiz-Fernández, J., Oliva, M., Nývlt, D., Cannone, N., García-Hernández, C., Guglielmin, M., Hrbáček, F., Roman, M., Fernández, S., López-Martínez, J., & Antoniades, D. (2019). Patterns of spatio-temporal paraglacial response in the AP region and associated ecological implications. *Earth-Science Reviews*, *192*, 379–402. https://doi.org/10.1016/j.earscirev.2019.03.014

Schimmelpfennig, I., Benedetti, L., Finkel, R., Pik, R., Blard, P. H., Bourlès, D., Burnard, P., & Williams, A. (2009). Sources of in-situ36Cl in basaltic rocks. Implications for calibration of production rates. *Quaternary Geochronology*, *4*, 441–461. https://doi.org/10.1016/j.quageo.2009.06.003

Schimmelpfennig, I., Benedetti, L., Garreta, V., Pik, R., Blard, P. H., Burnard, P., Bourlès, D., Finkel, R., Ammon, K., & Dunai, T. (2011). Calibration of cosmogenic 36Cl production rates from Ca and K spallation in lava flows from Mt. Etna (38° N, Italy) and Payun Matru (36°S, Argentina). *Geochimica et Cosmochimica Acta*, *75*, 2611–2632. https://doi.org/10.1016/j.gca.2011.02.013

Schimmelpfennig, I., Schaefer, J. M., Putnam, A. E., Koffman, T., Benedetti, L., Ivy-Ochs, S., Schlüchter, C., Arnold, M., Aumaître, G., Bourlès, D., Keddadouche, K., Team, A., & Schlüchter, C. (2014). 36Cl production rate from K-spallation in the European Alps (Chironico landslide, Switzerland). *Journal of Quaternary Science*, *29*, 407–413. https://doi.org/10.1002/jqs.2720

Schmidt, R., Mäusbacher, R., & Müller, R. (1990). Holocene diatom flora and stratigraphy from sediment cores of two Antarctic lakes (King George Island). *Journal of Paleolimnology*, *3*, 55–74. https://doi.org/10.1007/BF00209300

Seong, Y. B. A. E., Owen, L. A., Lim, H. S., Yoon, H. I., Kim, Y., Lee, Y. I. L., & Caffee, M. W. (2009). Rate of late quaternary ice-cap thinning on King George Island, South Shetland Islands, West Antarctica defined by Cosmogenic 36Cl surface exposure dating. *Boreas*, *38*, 207–213. https://doi.org/10.1111/j.1502-3885.2008.00069.x

Shahateet, K., Seehaus, T., Navarro, F., Sommer, C., & Braun, M. (2021). Geodetic mass balance of the South Shetland Islands ice caps, Antarctica, from differencing tanDEM-X DEMs. *Remote Sensing*, *13*(17), 3408. https://doi.org/10.3390/rs13173408

Shevenell, A. E., Ingalls, A. E., Domack, E. W., & Kelly, C. (2011). Holocene Southern Ocean surface temperature variability west of the Antarctic peninsula. *Nature*, *470*, 250–254. https://doi.org/10.1038/nature09751

Simms, A. R., Ivins, E. R., DeWitt, R., Kouremenos, P., & Simkins, L. M. (2012). Timing of the most recent Neoglacial advance and retreat in the South Shetland Islands, Antarctic peninsula: Insights from raised beaches and Holocene uplift rates. *Quaternary Science Reviews*, *47*, 41–55. https://doi.org/10.1016/j.quascirev.2012.05.013

Simms, A. R., DeWitt, R., Kouremenos, P., & Drewry, A. M. (2011). A new approach to reconstructing sea levels in Antarctica using optically stimulated luminescence of cobble surfaces. *Quaternary Geochronology*, *6*, 50–60. https://doi.org/10.1016/j.quageo.2010.06.004

Simms, A. R., Milliken, K. T., Anderson, J. B., & Wellner, J. S. (2011). The marine record of deglaciation of the South Shetland Islands, Antarctica since the last glacial maximum. *Quaternary Science Reviews*, *30*, 1583–1601. https://doi.org/10.1016/j.quascirev.2011.03.018

Small, D., Bentley, M. J., Jones, R. S., Pittard, M. L., & Whitehouse, P. L. (2019). Antarctic ice sheet palaeo-thinning rates from vertical transects of cosmogenic exposure ages. *Quaternary Science Reviews*, *206*, 65–80. https://doi.org/10.1016/j.quascirev.2018.12.024

Stone, J. O. (2000). Air pressure and cosmogenic isotope production. *Journal of Geophysical Research: Solid Earth*, *105*, 23753–23759. https://doi.org/10.1029/2000JB900181

Tatur, A., del Valle, R., Barczuk, A., & Martinez-Macchiavello, J. (2004). Records of Holocene environmental changes in terrestrial sedimentary deposits on King George Island, Antarctica; a critical review. *Ocean and Polar Research*, *26*, 531–537. https://doi.org/10.4217/OPR.2004.26.3.531

Toro, M., Granados, I., Pla, S., Giralt, S., Antoniades, D., Galán, L., Cortizas, A. M., Lim, H. S., & Appleby, P. G. (2013). Chronostratigraphy of the sedimentary record of Limnopolar Lake, byers peninsula, Livingston Island, Antarctica. *Antarctic Science*, *25*, 198–212. https://doi.org/10.1017/S0954102012000788

Turner, J., Colwell, S. R., Marshall, G. J., Lachlan-Cope, T. O. M. A., Carleton, A. M., Jones, P. D., Lagun, V., Reid, P. A., & Iagovkina, S. (2005). Antarctic climate change during the last 50 years. *International Journal of Climatology*, *25*, 279–294. https://doi.org/10.1002/joc.1130

Uppala, S. M., Kållberg, P. W., Simmons, A. J., Andrae, U., da Costa Bechtold, V., Fiorino, M., Gibson, J. K., Haseler, J., Hernandez, A., Kelly, G. A., Li, X., Onogi, K., Saarinen, S., Sokka, N., Allan, R. P., Andersson, E., Arpe, K., Balmaseda, M. A., Beljaars, A. C. M., … Woollen, J. (2005). The ERA-40 re-analysis. *Quarterly Journal of the Royal Meteorological Society*, *131*, 2961–3012. https://doi.org/10.1256/qj.04.176

Valle, R. A. D. E. L., Montalti, D., Inbar, M., Del Valle, R. A., Montalti, D., & Inbar, M. (2002). Mid-Holocene macrofossil-bearing raised marine beaches at potter peninsula, King George Island, South Shetland Islands. *Antarctic Science*, *14*, 263–269. https://doi.org/10.1017/S0954102002000081

Vieira, G., Bockheim, J., Guglielmin, M., Balks, M., Abramov, A. A., Boelhouwers, J., Cannone, N., Ganzert, L., Gilichinsky, D. A., Goryachkin, S., López-Martínez, J., Meiklejohn, I., Raffi, R., Ramos, M., Schaefer, C., Serrano, E., Simas, F., Sletten, R., & Wagner, D. (2010). Thermal state of permafrost and active-layer monitoring in the antarctic: Advances during the international polar year 2007-2009. *Permafrost and Periglacial Processes*, *21*, 182–197. https://doi.org/10.1002/ppp.685

Ward, G. K., & Wilson, S. R. (1978). Procedures for comparing and combining radiocarbon age determinations: A critique. *Archaeometry*, *20*, 19–31. https://doi.org/10.1111/j.1475-4754.1978.tb00208.x

Watcham, E. P., Bentley, M. J., Hodgson, D. A., Roberts, S. J., Fretwell, P. T., Lloyd, J. M., Larter, R. D., Whitehouse, P. L., Leng, M. J., Monien, P., & Moreton, S. G. (2011). A new Holocene relative sea level curve for the South Shetland Islands, Antarctica. *Quaternary Science Reviews*, *30*, 3152–3170. https://doi.org/10.1016/j.quascirev.2011.07.021

Yoon, H. I., Khim, B. K., Lee, K., Park, Y. H., & Yoo, K. C. (2006). Reconstruction of postglacial paleoproductivity in long Lake, King George Island, West Antarctica. *Polish Polar Research*, *27*, 189–206.

Yoon, H. I., Yoo, K. C., Bak, Y. S., Lim, H. S., Kim, Y., & Lee, J. I. (2010). Late holocene cyclic glaciomarine sedimentation in a subpolar fjord of the South Shetland Islands, Antarctica, and its paleoceanographic significance: Sedimentological, geochemical, and paleontological evidence. *Bulletin Geological Society of America*, *122*, 1298–1307. https://doi.org/10.3233/BD-160236

Zale, R., & Karlén, W. (1989). Lake sediment cores from the Antarctic peninsula and Surrounding Islands. *Geografiska Annaler Series A: Physical Geography*, *71*, 211–220. https://doi.org/10.1080/04353676.1989.11880288

How to cite this article: Oliva, M., Palacios, D., Fernández-Fernández, J. M., Fernandes, M., Schimmelpfennig, I., Vieira, G., Antoniades, D., Pérez-Alberti, A., García-Oteyza, J., & ASTER TEAM (2023). Holocene deglaciation of the northern Fildes Peninsula, King George Island, Antarctica. *Land Degradation & Development*, 1–18. https://doi.org/10.1002/ldr.4730